

MICROCOPY RESOLUTION TEST CHART
NATIONAL BUREAU OF STANDARDS-1963-A

AFOSR-TR- 86-0696

2

Scientific Report

on

"Studies of Optical Wave Front Conjugation and Imaging
Properties of Nematic Liquid Crystal Films"

[AFOSR 840375]

Approved for public release;
distribution unlimited.

Submitted to

Air Force Office of Scientific Research

Bolling Air Force Base

Washington, D.C. 20332

Attention: Lt. Col. Robert Carter, Jr.

By

Dr. Iam-Choon Khoo

Department of Electrical Engineering

Pennsylvania State University

University Park, PA 16802

June 1986

DTIC
ELECTRONIC
SEP 19 1986
S
A

AD-A172 089

DTIC FILE COPY

AIR FORCE OFFICE OF SCIENTIFIC RESEARCH (AFSC)
NOTICE OF TRANSMITTAL TO DTIC
This technical report has been reviewed and is
approved for public release IAW AFR 190-12.
Distribution is unlimited.
MARITON J. KETTER
Chief, Technical Information Division

REPORT DOCUMENTATION PAGE

1a. REPORT SECURITY CLASSIFICATION Unclassified			1b. RESTRICTIVE MARKINGS											
2a. SECURITY CLASSIFICATION AUTHORITY			3. DISTRIBUTION/AVAILABILITY OF REPORT Approved for public release, distribution unlimited											
2b. DECLASSIFICATION/DOWNGRADING SCHEDULE														
4. PERFORMING ORGANIZATION REPORT NUMBER(S)			5. MONITORING ORGANIZATION REPORT NUMBER(S) AFOSR-TR-86-0096											
6a. NAME OF PERFORMING ORGANIZATION Pennsylvania State U		6b. OFFICE SYMBOL <i>(If applicable)</i>	7a. NAME OF MONITORING ORGANIZATION AFOSR											
6c. ADDRESS (City, State and ZIP Code) Dept of Electrical Engineering University Park PA 16802			7b. ADDRESS (City, State and ZIP Code) same as 8c											
8a. NAME OF FUNDING/SPONSORING ORGANIZATION AFOSR		8b. OFFICE SYMBOL <i>(If applicable)</i> NE	9. PROCUREMENT INSTRUMENT IDENTIFICATION NUMBER AFOSR-84-0375											
8c. ADDRESS (City, State and ZIP Code) Bolling AFB DC 20332-6448			10. SOURCE OF FUNDING NOS. <table border="1" style="width: 100%; border-collapse: collapse;"> <tr> <th style="width: 25%;">PROGRAM ELEMENT NO.</th> <th style="width: 25%;">PROJECT NO.</th> <th style="width: 25%;">TASK NO.</th> <th style="width: 25%;">WORK UNIT NO.</th> </tr> <tr> <td style="text-align: center;">61102F</td> <td style="text-align: center;">2305</td> <td style="text-align: center;">B4</td> <td></td> </tr> </table>			PROGRAM ELEMENT NO.	PROJECT NO.	TASK NO.	WORK UNIT NO.	61102F	2305	B4		
PROGRAM ELEMENT NO.	PROJECT NO.	TASK NO.	WORK UNIT NO.											
61102F	2305	B4												
11. TITLE (Include Security Classification) "STUDIES OF OPTICAL WAVE FRONT CONJUGATION"														
12. PERSONAL AUTHOR(S) AND IMAGING PROPERTIES OF NEMATIC LIQUID CRYSTAL FILMS Dr. Iam-Choon Khoo														
13a. TYPE OF REPORT ANNUAL		13b. TIME COVERED FROM 15SEP84 TO 14SEP85		14. DATE OF REPORT (Yr., Mo., Day) June 86	15. PAGE COUNT DTIC ELECTE SEP 10 1986 A									
16. SUPPLEMENTARY NOTATION														
17. COSATI CODES <table border="1" style="width: 100%; border-collapse: collapse;"> <thead> <tr> <th style="width: 33%;">FIELD</th> <th style="width: 33%;">GROUP</th> <th style="width: 33%;">SUB. GR.</th> </tr> </thead> <tbody> <tr> <td> </td> <td> </td> <td> </td> </tr> <tr> <td> </td> <td> </td> <td> </td> </tr> </tbody> </table>			FIELD	GROUP	SUB. GR.							18. SUBJECT TERMS (Continue on reverse if necessary and identify by block number)		
FIELD	GROUP	SUB. GR.												
19. ABSTRACT (Continue on reverse if necessary and identify by block number) Optical nonlinearities of liquid crystals owing to laser induced molecular reorientation or laser induced thermal index change, were studied in the context of optical wave mixings and real time imagings. The basic mechanisms and the dynamics of the nonlinearities were studied in details in theories, and in experiments using lasers of various time scales and temporal characteristics. Quantitative documentation of nanosecond laser induced thermal grating was performed for the first time, and further established the optical imaging and switching capabilities of nematic liquid crystal film. The conversion of infra-red images to visible images via real-time optical wave mixing process was also demonstrated. The capability of optical four wave mixing to generate amplified reflection and self oscillation in nematic liquid crystal film was also demonstrated for the first time. Such a process will be useful for image processing as well as laser oscillator adaptive optica applications. In this period, new optical intensity switching effects using the transverse optical nonlinearity were also experimentally demonstrated, that will,														
20. DISTRIBUTION/AVAILABILITY OF ABSTRACT UNCLASSIFIED/UNLIMITED <input type="checkbox"/> SAME AS RPT. <input type="checkbox"/> DTIC USERS <input type="checkbox"/>			21. ABSTRACT SECURITY CLASSIFICATION											
22a. NAME OF RESPONSIBLE INDIVIDUAL Lt Col Robert W. Carter, Jr.		22b. TELEPHONE NUMBER (Include Area Code) 202-767-4931		22c. OFFICE SYMBOL AFOSR/NE										

~~Unclass~~

SECURITY CLASSIFICATION OF THIS PAGE

Abstract Cont'd

find applications in optical switching and power self limiting devices.

SECURITY CLASSIFICATION OF THIS PAGE

Table of Contents

	Page
Summary	2
I Introduction	3
II Research Accomplishments	6
III List of Publications	10
V Personnel	12
IV Reprints and Preprints (6)	13



Accession For	
NTIS GRA&I	<input checked="" type="checkbox"/>
DTIC TAB	<input type="checkbox"/>
Unannounced	<input type="checkbox"/>
Justification	
By	
Date	
App	
Dist	

A-1

Summary

Optical nonlinearities of liquid crystals owing to laser induced molecular reorientation or laser induced thermal index change, were studied in the context of optical wave mixings and real time imagings. The basic mechanisms and the dynamics of the nonlinearities were studied in details in theories, and in experiments using lasers of various time scales and temporal characteristics. Quantitative documentation of nanosecond laser induced thermal grating was performed for the first time, and further established the optical imaging and switching capabilities of nematic liquid crystal film. The conversion of infra-red images to visible images via real time optical wave mixing process was also demonstrated. The capability of optical four wave mixing to generate amplified reflection and self oscillation in nematic liquid crystal film was also demonstrated for the first time. Such a process will be useful for image processing as well as laser oscillator adaptive optics applications. In this period, new optical intensity switching effects using the transverse optical nonlinearity were also experimentally demonstrated, that will find applications in optical switching and power self limiting devices.

I Introduction

Current research and development in optical imaging and signal processing have largely employed the nonlinear optical and electro-optical properties of certain crystals and thin film devices. In combination with new novel nonlinear optical processes, and cw or pulsed lasers covering the UV to far IR spectrum, useful high resolution imaging system with aberration correction capability and other image processing capabilities, optical light modulators, switches and various signal processing devices and adaptive optics applications have emerged. Nevertheless, the number of useful nonlinear (or otherwise) optical materials for meeting these new application demands is relatively limited.

This proposal is devoted to a detailed study of the special nonlinear optical properties of liquid crystal films for optical wave front conjugation and in related four-wave mixing processes. The fabrication of stable, high optical quality liquid crystal thin film has been established for many years. Commercially, an ever increasing number of liquid crystal of wide ranging physical characteristics are becoming available. These basic advantages, together with the recently discovered extraordinarily large optical nonlinearities make liquid crystals an attractive candidate for nonlinear optical switches and devices. We anticipate that some of the processes under study will in fact find immediate applications.

There are two distinct basic mechanisms for nonlinearity in liquid crystal. One is the optical field induced reorientation of the axially birefringent nematics. Perhaps the most important characteristics of liquid crystals is their large optical anisotropy $\Delta\epsilon$ ($\Delta\epsilon = \epsilon_{11} - \epsilon_{\perp}$) is the dielectric constant for optical field parallel, and perpendicular to the director

(optical) axis of the liquid crystal, respectively. Typically $\Delta\epsilon$ ranges from 0.4 to 1. Recent discovery by this investigator that it is possible to induce director axis reorientation with relatively low power lasers (with intensities on the order of watts/cm²) had opened up a wide range of possibilities for nonlinear optical effects and applications. Most of the pioneer work have been conducted by this investigator in the past few years. Work done during the period supported by the Air Force Office of Scientific Research is detailed in the next section.

The other mechanism for optical nonlinearity is the naturally present high thermal index gradients of liquid crystal, especially near the nematic \rightarrow isotropic phase transition temperature T_c . At temperatures far from T_c , both dn_e/dT and dn_o/dT (where n_e and n_o are the extraordinary and the ordinary refractive indices, respectively) are already higher than most high thermal index materials (e.g. cyclohexane). Near T_c , the magnitudes of these two increase by more than an order of magnitude. Since many nonlinear processes, e.g. optical wave mixings, wave front conjugations, self-phase modulation...etc., depends on the laser induce thermal index changes, these effects can be observed in liquid crystals at much lower laser power (or energy). More importantly, since the required refractive index change can be achieved with high energy pulsed lasers, the (nonlinear) processes can also occur with a fast on-time.

Our proposed program is centered on four wave mixings and related optical processes based on these two nonlinearities. Our principle objective are to (i) quantitatively characterize the wave front conjugation performance of nematic liquid crystal film in the submillisecond require under pulsed laser illuminations and (ii) to quantitatively study the optical imaging capabilities of nematic films using cw or pulsed lasers, using light source of

visible or infra-red spectrum. To this end, our research during the first year of the Air Force Office of Scientific Research support has been extremely productive.

II Research Accomplishment

In the following paragraphs, we will summarize our research accomplishment into five broad categories. The related publications, conference presentations and other forms of research records are listed in the next section. A detailed plan for future work is described in the renewal proposal entitled "Studies of Optical Wave Front Conjugations, Imagings and Switching Properties of Liquid Crystals" that was submitted in July 1985 to the Air Force Office of Scientific Research.

During the period 8/15/84 to present date:

1. We have conducted a thorough review of the theory and experiments on the orientational optical nonlinearity of liquid crystals in their nematic phase. We have compared and contrasted the nonlinearity with those observed previously in the liquid phases. A detailed examination of their dynamics (rise - and decay - times) and how these dynamics are affected by various liquid crystalline parameters (like viscosity, temperature, elastic constants...etc) and geometrical configurations and laser intensity is performed. An important point that is borne out in actual experimentations is that the response of the liquid crystal reorientation can be faster if higher intensity lasers are used. Nanosecond response is possible with Megawatt/cm² optical intensity.

The extraordinarily large optical nonlinearity associated with director reorientation has also been utilized to gain further insights into several nonlinear optical processes like self-focusing, self phase modulation, optical bistability, nonlinear wave guiding and optical

wave mixings. We have also developed a theory for the nonlocal dependence of the director axis reorientation with respect to the incident laser spot size, and conducted experimental measurements that substantiated the theoretical results. These nonlocal dependence will be important in assessing the amount of cross talks in optical processing using multi-beams, and in the resolution limit in optical imaging processes.

The details of these research findings and the possibilities for future research work may be seen in the attached re/preprints.

2. We have also conducted a thorough theoretical analysis and experimental study of the basic mechanisms and the dynamics of laser induced thermal index change in nematic liquid crystals. In particular, we have performed a calculation based on current molecular theory of nematogen on both the ordinary and the extraordinary refractive index changes with temperature, and the index (holographic) grating associated with two laser beams mixings. Experimentally, we have employed nanosecond laser pulses to generate the thermal grating and studied its rise and decay time. Very interesting high frequency (GHz) interference effects associated with laser induced acoustic waves are observed in the first 100 ns of the rise part. The decay dynamics, and the anisotropy of the dynamics were found to be in agreement with the theoretical expectations. This detailed study has conclusively demonstrated that laser induced thermal grating and index change in nematic liquid can be a very useful mechanism for applications; future research on this is clearly called for.

The attached reprint from IEEE J. Quant Electronics discussed all these in greater details.

3. In line with the thermal grating studies reported in item 2 above, we have also looked into the quasi steady state case where the thermal grating is induced by laser pulses on the order of ms, on the order the thermal decay time constant. For this case, as discussed in the attached preprints, the grating associated with two beam mixings can be maximized if the grating spacing is large. In conjunction with the extraordinarily large thermal nonlinearity, we have observed for the first time wave front conjugation with gain in a nematic liquid crystal film, and the related self-oscillations, using low power cw visible laser. This opens up a rather exciting new area, e.g., the possibility of image amplification, ring oscillator amplifier, etc., associated with these two wave mixing processes. Moreover, the absorption constant of the liquid crystal can be increased with traces of dissolved dye that absorbs in the IR regime, and thus one can extend all these studies to IR lasers.

The attached preprint of an Applied Physics Letters (Nov. issue, 1985), presents more details on this subject, and on our contemplated future goals.

4. Related to items 2 and 3 is the process of so-called nondegenerate four wave mixing, whereby the real time holographic grating is generated with

lasers of one wavelength, and the image is reconstructed at another desired wavelength. We have, as an example, demonstrated the possibility of converting infra-red images to the visible. Obviously, the reverse is also possible. It is also possible to have an incoherent to coherent image conversion using a similar four wave mixing scheme, but it remains to be demonstrated. An interesting observation is that using liquid crystals "doped" with IR absorbing dyes, IR laser energies on the order of $1\text{mJ}/\text{cm}^2$ or so are sufficient for the wavelength conversion, and at a relatively fast time scale (nanoseconds on-time, microseconds off-time). The details of the IR \rightarrow visible image conversion process via four wave mixing is reported in the August issue of Applied Physics Letters (attached).

5. During this past year, we have also followed up on our previous research expertise in transverse self-phase modulation and conducted studies on some novel transverse switching processes. This includes optical power limiting and laser self-bending effects. The studies are in the preliminary stage but we have already obtained very interesting switching results.

A brief version of this was presented at the January SPIE Conference at Los Angeles. A more detailed description was published at the April issue (1986) Optics Letters (see reprints enclosed).

III List of Publications (Sept. 1984 - August 1985)

1. The mechanism and dynamics of transient thermal grating diffraction in nematic liquid crystal films I.C. Khoo and R. Normandin, IEEE J. Quantum Electronics QE21, 329 (1985).
2. Liquid crystals: nonlinear optical properties and processes I.C. Khoo and Y.R. Shen, Optical Eng. 24, P. 579 (1985).
3. Infra-red to visible image conversion capability of a nematic liquid crystal film.
I.C. Khoo and R. Normandin, Appl. Phys. Letts. 47, 350 (1985).
4. Wave front conjugation with gain and self-oscillation with a nematic liquid-crystal film.
I.C. Khoo, Appl. Phys. Letts. Nov. issue, 1985.
5. Transverse self-phase modulation optical bistability.
I.C. Khoo, Invited paper, Proceedings of 7th International Conference on Lasers and Applications (August 1985).
6. Passive optical self limiter using laser induced axially symmetric and asymmetric transverse self-phase modulations in a liquid crystal film. I.C. Khoo, G. Finn, R.R. Michael and T.H. Liu, Optics Letters 11, 227 (1986)
7. Nonlinear optical properties of liquid crystal films for optical imaging processes. I.C. Khoo, Opt. Eng. 25, 198 (1986).

IV Conference Presentations

1. Optical wave mixings in the mesophases of liquid crystals using nanosecond lasers. I.C. Khoo, Presented at the 1984 Annual Meeting of the Optical Society of America, October 1984.
2. Cavityless optical switching elements using nonlinear self-phase modulation. I.C. Khoo and T.H. Liu, Presented at the 1984 Annual Optical Society of America Meeting, October 1984.
3. Transverse self-phase modulation bistability in a nonlinear thin-film theory and experiment. I.C. Khoo, T.H. Liu and R. Normandin, International Conference on Lasers and Application -- Lasers '84, November 1984.
4. Optical bistability of a dielectric cladded thin film near the total internal reflection state -- theory and experiment -- I.C. Khoo and J.Y. Hou. Presented at the Conference on Lasers and Electro-Optics, 1985.
5. Infra-red to visible image conversion using four-wave mixing in a liquid crystal film. I.C. Khoo and R. Normandin. Presented at the Conference on Lasers and Electro-Optics, 1985.
6. Nondegenerate four wave mixing and IR to visible image conversion in liquid crystal film. I.C. Khoo et al, Presented at the 1985 Annual Meeting of Optical Society of America, Washington, D.C. (1985).

7. Nonlocal transverse dependence of liquid crystal director reorientation and nonlinearity induced by a laser beam. I.C. Khoo et al, Presented at the 1985 Annual meeting of the Optical Society of America, Washing D.C.
8. Saturation and nonlocal effect in transverse self-phase modulation bistability. I.C. Khoo et al, Presented at the 1985 Annual Meeting of the Optical Society of America, Washington, D.C.
9. Laser self power limiting and self bending effect using nematic films. I.C.Khoo et al, Presented at the Jan.SPIE technical Conference, LA.CA.
10. Wave front conjugation with gain in a nematic liquid crystal film. I.C.Khoo, Presented at the Jan.SPIE Technical Conference, LA, CA.

Nonlinear optical properties of liquid crystals for optical imaging processes

I. C. Khoo, MEMBER SPIE

The Pennsylvania State University
Department of Electrical Engineering
University Park, Pennsylvania 16802

Abstract. We present an account of two recently observed nonlinear optical imaging processes, wavefront conjugation and infrared-to-visible image conversion, in liquid crystal films. We include discussion of dynamics, efficiency, resolution, aberration correction, and noise removal in these two processes.

Subject terms: optical information processing; lasers; thermal indexing; liquid crystals; reorientation; nonlinear imaging.

Optical Engineering 25(2), 198-201 (February 1986).

CONTENTS

1. Introduction
2. Wavefront conjugation
3. Infrared-to-visible image conversion
4. Conclusion
5. Acknowledgments
6. References

1. INTRODUCTION

The theory and practice of liquid crystal director axis reorientations, and the associated electro-optical birefringence, by a dc or low frequency ac field have been established for many years. Various optical imaging, image processing, modulation, switching, and display devices are based on these rather simple physical effects. When integrated with other thin-film materials (semiconductors, photoconductors, metallic films, etc.), liquid crystals become one of the most versatile optical materials that find application in an ever-increasing array of optical information processing systems.¹

Recently, the feasibility of employing moderate power lasers to induce molecular reorientation in liquid crystals has been demonstrated.² All three mesophases (nematics, smectics, and cholesterics) exhibit extraordinarily large optical nonlinearity associated with the director axis reorientation. To date, however, the most conclusive theories and experiments have been performed in nematics, which are also the most used materials for liquid crystal optical devices.³ There are two basic types of optical nonlinearities in nematics: (1) optically induced refractive index change associated with director axis reorientation and (2) thermal indexing effect. These nonlinearities have been studied in the context of self-focusing,⁴ degenerate four-wave mixing,⁵ self-phase modulations,⁶ bistability,⁷ and optical switching⁸ and have been reviewed in a recent article by Khoo and Shen.²

In this paper, we concentrate on two recently observed nonlinear optical processes that bear on optical imaging applications, namely, wavefront conjugation and IR-to-visible image conversion. We discuss details that are not

included in preliminary reports. Specifically, we address the conditions necessary for observing the effects, the diffraction efficiencies, rise and fall times, and other pertinent imaging characteristics.

2. WAVEFRONT CONJUGATION

The theory of wavefront conjugation, an example of degenerate four-wave mixing processes, has been established for many years.⁹ An experimental setup for wavefront conjugation is shown schematically in Fig. 1(a). The object beam and the reference beam interfere to induce an index grating (a transient hologram) on the liquid crystal film by means of either the orientational or the thermal nonlinearity. The reconstructing beam is retroreflected from the reference beam, and the image-bearing generated fourth wave traverses back along the object beam path. There are several significant advantages of this type of real-time imaging process, a few of which are high resolution, reflections with gain, and aberration correction capability.

In an earlier wavefront conjugation experiment,¹⁰ we showed that because of the extremely large optical nonlinearity of liquid crystals, cw lasers of a few W/cm² intensity suffice for visible phase conjugation results. We have also demonstrated phase-aberrated corrections. More recently, we have succeeded in using a spatially partially coherent cw laser to remove the coherent noise that inevitably accompanies the use of lasers for imaging. In nematic film, the problem is particularly severe owing to extremely high scatterings from director axis fluctuations. Figure 1(b) is an example of an extremely degraded (by the coherent artifacts) reconstructed image beam in a wavefront conjugation experiment using a coherent laser. The photograph is taken at a temperature near T_c , the transition temperature. At temperatures far from T_c , the noise is less overwhelming but still very severe and is compounded by the ever-present noise from random scatterings in the optical system.

Two methods of removing the coherent noise in phase conjugation have been demonstrated to be quite successful. In the method employed by Huignard et al.,¹¹ a diffuser plate is placed in the path of the object beam (pulsed laser), and multiple exposures are taken for various settings of the diffuser plate. In our collaborative study with Leith et al.,¹² the

Invited Paper MD-101 received June 29, 1985; revised manuscript received Oct. 4, 1985; accepted for publication Oct. 7, 1985; received by Managing Editor Nov. 18, 1985.

© 1986 Society of Photo-Optical Instrumentation Engineers.

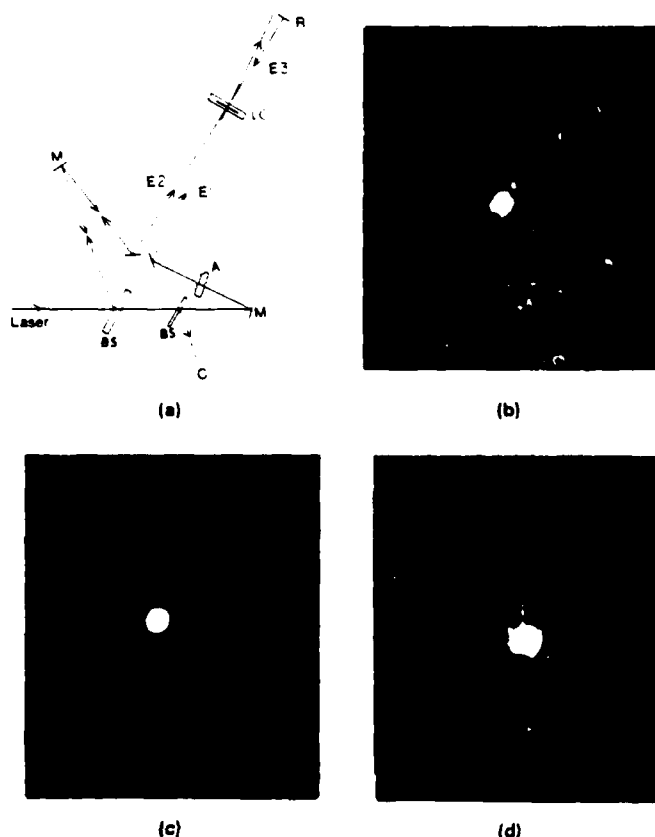


Fig. 1. Wavefront conjugation. (a) Experimental setup. BS: beam splitter. M: mirror. R: total reflector. S: sample. E_2 : reference beam. E_1 : object beam. E_3 : reconstruction beam. A: aberrator. C: image. (b) Image beam reconstructed with coherent laser. (c) Image beam reconstructed with spatially incoherent laser. (d) Aberrated beam.

cw laser was first rendered spatially partially incoherent by collimation through a rotating ground glass. Because the rise time of the conjugation process with cw laser illumination is slow, the incident laser beam is practically averaged over many settings of the rotating ground glass, so that a *single* exposure recording of the image beam will suffice. As shown in Fig. 1(c) of the reconstructed beam and Fig. 1(d) of the aberrated beam, the technique both preserves the aberration correction capability and removes coherent noise.

Recently we demonstrated¹³ that wavefront conjugation with a nanosecond pulsed laser is feasible using the thermal nonlinearity. Near T_c , four-wave mixing with moderate laser energy (≤ 1 mJ) is possible, with microsecond response (rise and fall). We are currently investigating various means of achieving coherent-noise-free wavefront conjugation imaging.

The diffraction efficiency for wavefront conjugation and the related infrared-to-visible image conversion at the phase-matched Bragg's condition depend principally on the magnitude of the induced index grating on $(\mathbf{K}_1 - \mathbf{K}_2)$ between the reference beam (at \mathbf{K}_1) and the object beam (at \mathbf{K}_2). In the absence of loss, the maximum diffraction efficiency R_{\max} is given roughly by $R_{\max} \approx (\mathbf{K}^2/4\eta^2)(\Delta\eta)^2d^2$, where d is the thickness of the film (or interaction length, whichever is shorter), \mathbf{K} is the magnitude of \mathbf{K}_1 and \mathbf{K}_2 , and η is the average refractive index. The magnitude of $\Delta\eta$ depends on which nonlinearity is responsible for the wave mixing process.

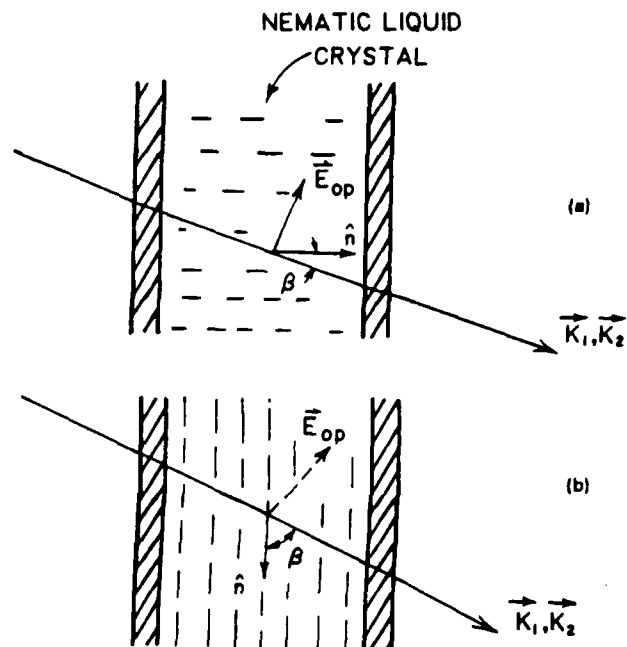


Fig. 2. Schematics of laser propagation in (a) a homeotropic nematic liquid crystal film and (b) a planar nematic film. \mathbf{K}_1 and \mathbf{K}_2 are the propagation wave vectors; \vec{E}_{op} is the optical field vector. The two laser beams lie in a plane perpendicular to the paper and intersect at a wave-mixing angle on the film.

For orientational nonlinearity, $\Delta\eta(\mathbf{K}_1 - \mathbf{K}_2)$ has been calculated¹⁴ for the homeotropic and planar nematic films, as depicted in Fig. 2. A unique characteristic of nematic nonlinearity is that it is a collective phenomenon; it is extremely dependent on the boundary forces or torques. The optical torques at the interference intensity maxima must overcome not only the elastic restoring torque from the boundary plates, where molecules are rigidly anchored, but also torques from molecules situated at the intensity minima.¹⁴ The torque is inversely proportional to the characteristic length; in this case, the two characteristic lengths are the film thickness d and the grating constant $\lambda(\mathbf{K}_1 - \mathbf{K}_2)$. The smaller these lengths, the higher is the optical intensity needed to induce the same amount of $\Delta\eta$, and therefore the lower is the diffraction efficiency. This has been verified in our experiments reported in Ref. 14, where details of the experimental results are also given.

The magnitude of $\Delta\eta$ due to laser heating depends to a large extent on the temporal characteristics of the laser. If cw lasers are used, then the thermal diffusion process during the grating buildup has to be accounted for. This is quite complicated and has hitherto not been addressed. On the other hand, if pulsed lasers (with pulse lengths shorter than the smallest diffusion time constant) are used, the analysis is simpler. In this case, $\Delta\eta$ depends simply on the heat capacity of the nematics, on the absorption constant of the nematics at the laser wavelength used, and to a great extent on the temperature (whether close to or far from T_c). Details of these for the nematic PCB (4-cyano-4-pentylbiphenyl) for pulsed lasers at 5145 Å have been presented.¹⁵ Typical values are $\Delta\eta \approx 10^{-4}$ for laser energies of approximately 20 mJ/mm² at $T_c - T \approx 14^\circ$. Near T_c , however, laser fluence on the order of 1 mJ will generate the same diffraction efficiency.

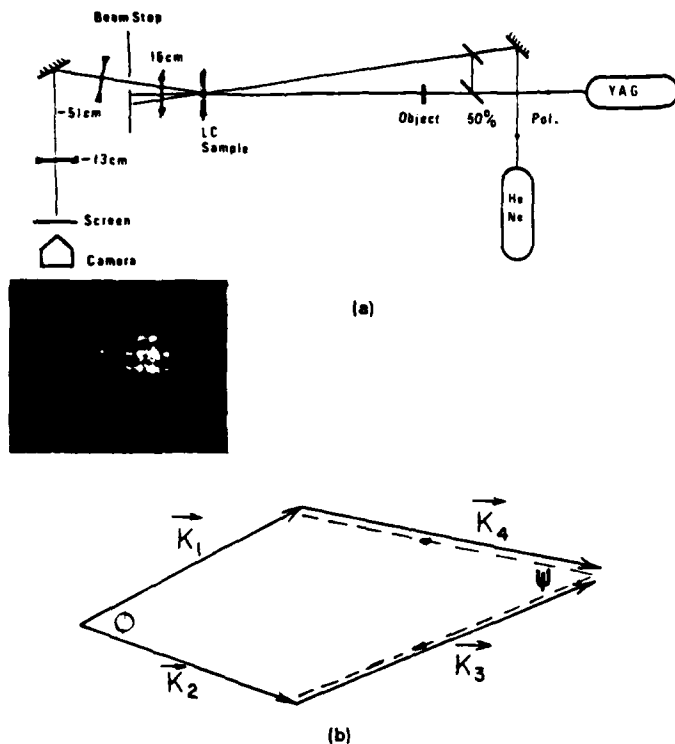


Fig. 3. Infrared-to-visible image conversion. (a) Experimental setup. (b) Phase matching of the four interacting waves. Dotted lines show the configuration used in Ref. 18. \vec{K}_1 : reference beam. \vec{K}_2 : object beam. \vec{K}_3 : reconstruction beam. \vec{K}_4 : image beam.

The rise and fall times of these nonlinear processes depend on several factors. In the orientational process, the rise time τ_{on} and fall time τ_{off} are given by expressions similar to those involving dc fields, with the optical field E_{op} replacing the dc field E_{dc} , and with the appropriate values for the dielectric anisotropies.^{2, 16} Because the optical field can make an arbitrary angle with the director axis, depending on the laser propagation direction, the rise time is also dependent on the configuration. In general, the smaller the grating constant (or thickness of the film, whichever is smaller), the faster is the response. τ_{on} and τ_{off} are proportional to λ^2 (or d^2), greater than the viscosity, and inversely proportional to the elastic constant, as we will presently see.

More specifically, consider the four-wave mixing geometry depicted in Fig. 2(a) or 2(b). Because the film is thin (50 μm or so) and the beam sizes in all the wave mixing experiments are much larger (on the order of millimeters), the two beams can be assumed to be plane waves. Their interference, therefore, sets up a grating in the y direction, with grating wave vector $\vec{K}_1 - \vec{K}_2$ and a grating constant λ ($\lambda = 2\pi/|\vec{K}_1 - \vec{K}_2|$). The reorientational angle θ thus possesses spatial variation in both the z and y directions (see Ref. 14). Using a simplifying one-elastic constant approximation, the dynamics of the process may be described by¹⁵

$$\gamma \frac{d\theta}{dt} = K \left(\frac{d^2\theta}{dy^2} + \frac{d^2\theta}{dz^2} \right) + \frac{\Delta\epsilon E_{op}^2}{4\pi} \left[(\cos 2\beta)\theta + \frac{\sin(2\beta)}{2} \right]. \quad (1)$$

If the optical field term is smaller than the elastic term, then since $\theta(y) \approx \sin[(2\pi/\lambda)y]$ and $\theta(z) \approx \sin[(\pi/d)z]$, and following the usual analysis,¹⁶ one gets a response time (rise or fall)

$$\tau \approx \frac{\gamma}{K \left[\left(\frac{2\pi}{\lambda} \right)^2 + \left(\frac{\pi}{d} \right)^2 \right]} \quad (2)$$

On the other hand, if the optical term is much larger than the elastic term

$$\tau_{on} \approx \frac{4\pi\gamma}{\Delta\epsilon E_{op}^2 \cos(2\beta)} \quad (3)$$

One interesting possibility is that the rise time can be decreased with the use of high intensity lasers. Nanosecond laser-induced molecular reorientation has been demonstrated by Hsiung et al.¹³ The decay time, however, is at best on the order of a few ms for d or λ on the order of a few μm . In the case of thermal grating, the rise time is on the order of the laser pulse length. The fall time depends on the heat diffusion process, the sample thickness, the grating constant, and the diffusion constant.¹⁷ Decay times on the order of 50 to 100 μs were observed in our experiment involving λ on the order of 20 μm .

3. INFRARED-TO-VISIBLE IMAGE CONVERSION

Using a thin-film geometry, or the phase-matched Bragg scattering configuration, it is possible to create a holographic phase grating with reference and object beam at one wavelength and reconstruction and image beam at another wavelength. An example of this special case of four-wave mixing is the so-called infrared-to-visible image conversion, where the object and reference beams are in the infrared, and the reconstruction and the image beams are in the visible [Fig. 3(a)]. There is obvious practical usefulness of such an image conversion process. As detailed by Martin and Hellwarth,¹⁸ this four-wave mixing process can also yield high image resolution capability. Typically, the number of resolution elements is on the order of 10^4 or better.

The resolution of the imaging process obviously depends on the relative configurations between the various interacting beams. The geometry employed by Martin and Hellwarth is of the "folded" or "wavefront conjugation-like" type [see Fig. 3(b)], whereas the geometry we used is the "forward" wave-mixing type. In both cases, the angle ψ is the Bragg scattering angle. In our configuration the amount of variation in ϕ (the angle between \vec{K}_1 and \vec{K}_2) that would still allow for phase matching (i.e., $\Delta k l < \pi$) is given by $2\pi\phi\delta\phi \approx 4\pi^2 [K_1 d |1 + (K_1/K_3)|]^{-1}$. The diffraction solid angle of the object beam, which subtends on area A on the sample, is given by $\phi_D = 4\pi^2/K_1^2 A$. This gives the number of resolution elements $N \approx \delta\phi/\phi_D$ as

$$N \approx \frac{AK_1}{l|1 + (K_1/K_3)|} \quad (4)$$

This differs from N for Fig. 3(b) (dotted line) by the denominator.¹⁸ Since K_1 and K_3 are quite different for infrared-to-visible conversion, this difference in the denominator amounts to a factor of unity in N . For very nonlinear material (e.g., liquid crystals), the use of a thin film (small d) will increase the resolution capability considerably more than this unity factor between the two types of geometry.

Two unique characteristics of nematics make them far superior to the materials (mostly organic liquids doped with

IR-absorbing dyes) employed by Martin and Hellwarth. One is the unusually large $d\eta/dT$ of nematics, especially near T_c , where both the ordinary and extraordinary $d\eta/dT$'s are about two orders of magnitude larger than for most liquids of high thermal index. The other, more important characteristic is the unusually large reorientational nonlinearity, which is non-wavelength-selective; that is, any infrared lasers can be used. The basic mechanism for infrared-to-visible image conversion is the formation of the grating by the IR beams. Therefore, the dynamics and magnitude of the grating formed are the same as discussed in the preceding section.

Using the experimental setup of Fig. 3(a), we have demonstrated the feasibility of employing either kind of nonlinearity for infrared-to-visible image conversion. The infrared laser used is from a Nd:YAG, in single-pulsed (thermal) or high repetition rate pulsed (for quasi cw reorientation process) modes. The photograph inset in the figure is a typical visible reconstructed image of the wire mesh (infrared illuminated object). In general, a very good quality image can be reconstructed, with a diffraction efficiency on the order of a few percent. We found that traces of IR-absorbing dyes (Kodak #14015) dissolved in the liquid crystal help reduce the required laser energies (to approximately 1 mJ/cm^2) for visible diffraction. This is because pure PCB, like most other liquid crystals, does not absorb appreciably at $1.06 \mu\text{m}$. For optimal thermal effect, therefore, "doping" with dyes with appropriate spectral absorption characteristics is needed. We are currently employing other infrared light sources to ascertain the general characteristics, and also some specific details, concerning image conversion in nematic and other mesophases of liquid crystals.

4. CONCLUSION

We have briefly discussed two four-wave-mixing-based imaging applications of nematic liquid crystal films. The underlying thermal and reorientational nonlinearities are uniquely large and versatile. It is obvious that other nonlinear optical processes, such as opto-optical modulations, optical switchings, and many real-time image processings, can also be realized using nematic films. We anticipate reporting the

results of these studies in the near future.

5. ACKNOWLEDGMENTS

This research is supported by grants from the National Science Foundation (ECS 8415387) and the Air Force Office of Scientific Research (AFOSR 840375).

6. REFERENCES

1. See, for example, B. Bahadur, *Mol. Cryst. Liq. Cryst.* 109, 3 (1984); see also U. Efron, S. T. Wu, J. Grinberg, and L. D. Hess, *Opt. Eng.* 24(1), 111 (1985) and references therein on the use of Hughes liquid crystal light valves.
2. I. C. Khoo and Y. R. Shen, *Opt. Eng.* 24(4), 579 (1985) and references therein.
3. See, for example, B. Bahadur, *Mol. Cryst. Liq. Cryst.* 109, 3 (1984).
4. I. C. Khoo, S. L. Zhuang, and S. Shepard, *Appl. Phys. Lett.* 39, 937 (1981).
5. I. C. Khoo and S. L. Zhuang, *Appl. Phys. Lett.* 37, 3 (1980); I. C. Khoo, *Phys. Rev. A* 25, 1040 (1982); S. D. Durbin, S. M. Arakelian, and Y. R. Shen, *Opt. Lett.* 7, 145 (1982).
6. S. D. Durbin, S. M. Arakelian, and Y. R. Shen, *Opt. Lett.* 6, 411 (1981); N. F. Pilipetski, A. V. Sukhov, N. V. Tabiryan, and B. Ya Zel'dovich, *Opt. Commun.* 37, 280 (1981).
7. I. C. Khoo, *Appl. Phys. Lett.* 41, 909 (1982); M. M. Cheung, S. D. Durbin, and Y. R. Shen, *Opt. Lett.* 8, 39 (1983); I. C. Khoo, J. Y. Hou, R. Normandin, and V. C. Y. So, *Phys. Rev. A* 27, 3251 (1983).
8. I. C. Khoo, *Appl. Phys. Lett.* 40, 645 (1982); I. C. Khoo and J. Y. Hou, *J. Opt. Soc. Am. B* 2, 761 (1985).
9. See, for example, *Optical Phase Conjugation*, R. Fisher, ed., Academic Press, New York (1983); see also, J. F. Reintjes, *Nonlinear Optical Parametric Processes in Liquids and Gases*, Academic Press, New York (1983).
10. I. C. Khoo and S. L. Zhuang, *IEEE J. Quantum Electron.* QE18, 246 (1982).
11. J. P. Huignard, J. P. Herriau, P. Aubourg, and E. Spitz, *Opt. Lett.* 4, 21 (1979).
12. E. N. Leith, H. Chen, Y. S. Cheng, G. J. Swanson, and I. C. Khoo, *Proc. 5th Rochester Conference on Coherence and Quantum Optics* (June 1983), Plenum Press, New York (1984).
13. I. C. Khoo and R. Normandin, presented at the 1983 Annual Meeting of the Optical Society of America, New Orleans; see also H. Hsiung, L. P. Shi, and Y. R. Shen, *Phys. Rev. A* 30, 1453 (1984) for molecular reorientation with ns laser pulses.
14. I. C. Khoo, *Phys. Rev. A* 27, 2747 (1983).
15. I. C. Khoo, *Phys. Rev. A* 25, 1636 (1982); I. C. Khoo, *Phys. Rev. A* 26, 1131 (E) (1982); I. C. Khoo, *Phys. Rev. A* 25, 1040 (1982).
16. See, for example, P. G. deGennes, *The Physics of Liquid Crystals*, Oxford University Press, Oxford (1974).
17. I. C. Khoo and R. Normandin, *IEEE J. Quantum Electron.* QE21, 329 (1985).
18. G. Martin and R. W. Hellwarth, *Appl. Phys. Lett.* 34, 371 (1979). □

Liquid crystals: nonlinear optical properties and processes

I. C. Khoo

The Pennsylvania State University
Department of Electrical Engineering
University Park, Pennsylvania 16802

Y. R. Shen

University of California
Department of Physics
Berkeley, California 94720

Abstract. Liquid crystals as nonlinear optical materials are reviewed. Potential applications of these materials in wave mixing, phase conjugation, and optical bistability are discussed. The extremely large optical nonlinearity and the slow response time of these materials make them unique for studies of some highly nonlinear optical processes and their dynamic characteristics.

Subject terms: nonlinear optics; liquid crystals; reorientation; director axis; thermal index; wave mixing; phase conjugation; optical switching.

Optical Engineering 24(4), 579-585 (July/August 1985).

CONTENTS

1. Introduction
2. Optical nonlinearity of liquid crystals
3. Nonlinear optical effects in liquid crystals
 - 3.1. Harmonic generation
 - 3.2. Degenerate wave mixing and phase conjugation
 - 3.3. Self-focusing and self-phase modulation
 - 3.4. Optical bistability
4. Conclusion
5. Acknowledgments
6. References

1. INTRODUCTION

Liquid crystalline materials are generally composed of highly anisotropic molecules. Strong correlation in the orientations of such molecules can lead to the mesomorphic phases in which the molecules are orderly aligned and the medium behaves like an anisotropic fluid.^{1,2} The degree of molecular alignment as well as the direction can easily be changed by external perturbation.^{1,2} As a result, liquid crystals form a unique class of optical materials that have attracted much attention in the past 15 years. They are strongly birefringent and exhibit huge electro- and magneto-optical effects. Therefore, they have been used in practical applications as sensing, display, and memory devices.^{3,4}

Liquid crystals are also highly nonlinear.^{5,6} Since they differ from ordinary organic liquids only in molecular arrangement, the electronic contribution to the optical nonlinearity in such materials is not expected to be very different from those of ordinary liquids. Optical-field-induced molecular reorientation is, however, much more significant in liquid crystals because of the strong molecular correlation.

As far as field-induced reorientation through induced dipoles on molecules is concerned, dc and optical fields are basically equivalent aside from dispersion. In the mesomorphic phases, a dc field of ~ 100 V/cm is often sufficient to induce a significant reorientation of the molecular alignment, leading to an average refractive index change as large as ~ 0.01 to 0.1 . The corresponding optical beam intensity is only ~ 100 W/cm², which is readily obtainable from a cw argon laser. Such a high optical nonlinearity is not easily found in other materials and renders liquid crystals ideal for studies of nonlinear optical effects resulting from laser-induced refractive index changes. The rather unique features of liquid crystals as nonlinear optical media are that the samples are inexpensive and easy to prepare, the induced refractive indices are highly anisotropic, and the response times are very slow. Laser heating of liquid crystals in the mesophases can also lead to a change in the optical anisotropy. The response times of the laser-induced thermal effect and the laser-induced molecular reorientation are, however, quite different.

Although liquid crystals are birefringent in the mesophases, they are generally centrosymmetric (except in the cholesteric phase, where the helical molecular arrangement is weakly centrosymmetric.) Therefore, in such a medium, second-order nonlinear optical processes are forbidden and only third-order processes have been studied extensively. Most of the work has concentrated on studying nonlinear optical effects arising from the optical-field-induced refractive indices in liquid crystals. These studies have included self-focusing,⁷⁻¹⁰ self-phase modulation,^{11,12} degenerate wave mixing,¹³⁻¹⁶ phase conjugation,¹⁷ and optical bistability.¹⁸⁻²¹ The slow response of liquid crystals, though detrimental from the practical device point of view, makes transient studies of these effects fairly easy and interesting and provides some new features to these otherwise well-known nonlinear optical phenomena.^{7-10, 18-21}

In the following sections, we first present a general description of the physical mechanisms giving rise to the optical nonlinearity in the various phases of liquid crystals and then briefly discuss a number of nonlinear optical processes that have been observed in liquid crystals and their possible applications.

Invited Paper NO-105 received Jan. 8, 1985; revised manuscript received Feb. 13, 1985; accepted for publication Feb. 13, 1985; received by Managing Editor April 8, 1985.
© 1985 Society of Photo-Optical Instrumentation Engineers.

2. OPTICAL NONLINEARITY OF LIQUID CRYSTALS

The electronic structure of liquid crystals is mainly dominated by that of individual molecules. The electronic contribution to optical nonlinearity in liquid crystals is therefore essentially the same as that in liquids. It is generally not exceptionally large, and so we will not dwell on it here. Instead, we shall discuss only optical nonlinearity arising from molecular motion, namely, molecular reorientation and laser-induced thermal effect.

Consider first a liquid crystal in the isotropic phase in which molecules are randomly oriented. In the presence of a linearly polarized light, the molecules are partially aligned by the optical field. The degree of alignment is usually described by the so-called orientational order parameter Q (with $Q = 0$ and $Q = 1$ referring to random distribution and perfect alignment, respectively). We can define Q in terms of the optical susceptibility tensor χ .^{22,23} Assuming that the field E is along x , we have

$$\chi_{xx} = \bar{\chi} + \frac{2}{3} \Delta\chi_0 Q, \quad (1)$$

$$\chi_{yy} = \chi_{zz} = \bar{\chi} - \frac{1}{3} \Delta\chi_0 Q,$$

where $\bar{\chi} = (\chi_{xx} + \chi_{yy} + \chi_{zz})/3$ is the average linear susceptibility of the medium and $\Delta\chi_0$ is the anisotropy when the molecules are perfectly aligned ($Q = 1$). In the isotropic case, the optically induced Q is expected to be much smaller than one and can be shown to be of the form

$$Q \propto \frac{\Delta\chi_0 |E|^2}{T - T^*}. \quad (2)$$

Here, T^* is a fictitious second-order phase transition temperature that is somewhat below the actual isotropic-mesomorphic transition temperature T_{NI} ($T_{NI} - T^*$ is often less than 1 K). Thus, Q should diverge with $(T - T^*)^{-1}$ as T approaches T_{NI} . Such a pretransitional behavior is commonly known as critical divergence. Physically, this happens because the molecular correlation begins to set in as T approaches T^* . The changes in the refractive indices, $\Delta n_{xx} = -2\Delta n_{yy} = -2\Delta n_{zz} = (8\pi/3)\Delta\chi_0 Q$, are directly proportional to Q and hence to $(T - T^*)^{-1}$.

The above critical characteristic of liquid crystals has been verified experimentally.^{22,23} As an example, Fig. 1(a) shows that $\delta n = n_{xx} - n_{yy}$ of *p*-methoxy-benzylidene *p*-*n* butylaniline (MBBA) indeed varies with $(T - T^*)^{-1}$ as T approaches T_{NI} . [In the figure β is defined as $(n/\pi|E|^2)\delta n$ with $n = (n_{xx} + n_{yy} + n_{zz})/3$.] Because of critical divergence, $\delta n/|E|^2$ becomes as large as 10^{-9} esu even at $T - T_{NI} = 5$ K, which is almost 100 times larger than that of CS_2 . Generally associated with critical divergence is the critical slowing-down behavior; that is, the response time τ of δn is also proportional to $(T - T^*)^{-1}$, as shown in Fig. 1(b) for MBBA. At $T - T_{NI} = 5$ K, τ becomes as long as 100 ns. We can define a figure of merit $f = \Delta n_{xx}/|E|^2 \tau = (2\pi/3n)\beta/\tau$ to describe the strength of a nonlinear medium in practical applications when both the magnitude and the speed of response of Δn are important. For liquid crystals in the isotropic phase, we find

$$f \propto \frac{(\Delta\chi)^2}{\nu}. \quad (3)$$

where ν is a viscosity coefficient. For example, we have from Fig. 1, $f \approx 6 \times 10^{-3}$ esu/s.

In the mesophases, molecules are highly correlated. The optical field is no longer strong enough to modify the degree of molecular alignment in any appreciable sense, but it is strong enough to reorient the direction of molecular alignment. This is quite analogous to the reorientation of magnetization of a ferromagnetic domain by an

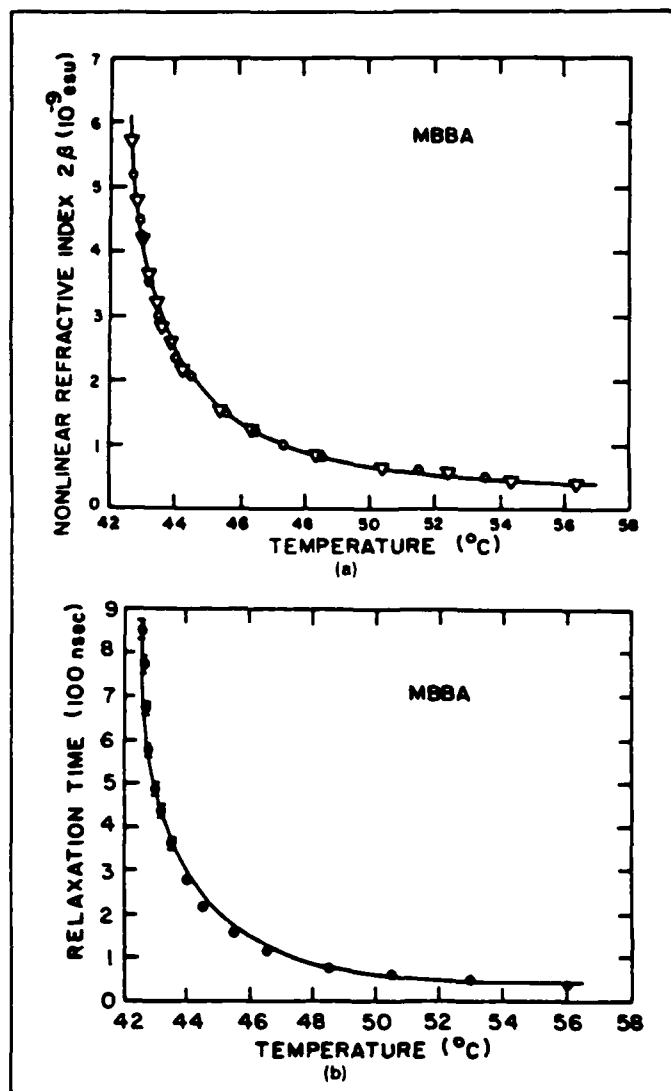


Fig. 1. (a) Nonlinear refractive index as a function of temperature for MBBA. The Δ are experimental data from optical Kerr measurements, and the \circ are experimental data from ellipse-rotation measurements. The solid curve is given by $5.4 \times 10^{-9}/(T - T_c)$ with 314.7 K. (b) Relaxation time τ_1 of the order parameter as a function of temperature for MBBA. The solid curve is the theoretical curve, and the dots are the experimental data points. (After Refs. 22 and 23.)

applied magnetic field. Because of the correlated molecular response (or the correlated spin response in the ferromagnetic case), the resulting change in the refractive indices (or effective magnetic susceptibility in the ferromagnetic case) is extremely large but slow. Realizing that the dc and optical fields are equivalent in orienting the molecules if no permanent dipole is present, we know that a laser intensity of ~ 250 W/cm² ($E = 300$ V/cm) is capable of inducing an average refractive index change of 0.01 to 0.1 in a nematic film,²⁴⁻³¹ but the response time can be more than a few seconds.

Detailed theoretical and experimental studies of optical-field-induced reorientation of molecular alignment have been carried out on homeotropic nematic films (i.e., molecular alignment perpendicular to the film) with extraordinary laser beams.²⁴⁻³¹ The direction of molecular alignment (known by the director) should obey the Euler equation derived from minimization of the free energy of the system. Let $\theta(z)$ be the angle the director makes with the surface normal at the position z in the film. (see Fig. 2). Then, we have³²

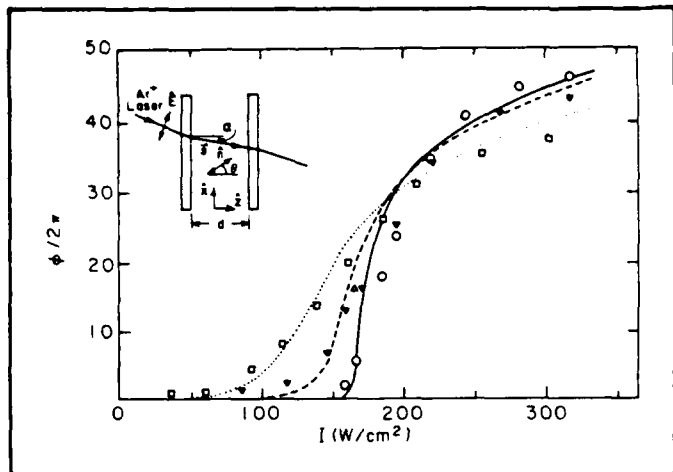


Fig. 2. Experimental data and theoretical curves for the phase shift $\Delta\phi$ induced in a 250 μm , homeotropically aligned, 5CB film by an Ar^+ laser beam at different angles α : circles and solid curve, $\alpha = 0^\circ$; solid triangles and dashed curve, $\alpha = 3^\circ$; squares and dotted curve, $\alpha = 11^\circ$. Inset shows the experimental geometry.

$$\frac{\partial\theta}{\partial z} = \pm \left[\frac{G(\theta) - G(\theta_m)}{H(\theta)} \right]^{1/2}, \quad (4)$$

where

$$G(\theta) = - \left[\frac{\epsilon_{\parallel}(\epsilon_{\parallel} - \epsilon_{\perp} \sin^2 \alpha)}{\epsilon_{\parallel}^2 - (\epsilon_{\parallel} - \epsilon_{\perp}) \epsilon_{\perp} \sin^2 \alpha} \right]^{1/2} \frac{1}{c} (1 - \epsilon_{\perp} \sin^2 \alpha)^{1/2}, \quad (5)$$

$$H(\theta) = \frac{1}{2} (K_{11} \sin^2 \theta + K_{33} \cos^2 \theta),$$

where ϵ_{\parallel} and ϵ_{\perp} are the optical dielectric constants parallel and perpendicular to the director, respectively, I is the incident laser beam intensity, α is the incident beam angle measured in the medium, and K_{11} and K_{33} are the splay and bend elastic coefficients, respectively. The solution of Eq. (4) is subject to the boundary condition $\theta = 0$ at $z = 0$ and $z = d$. If a normally incident probe beam is now used to measure the reorientation, it should experience a local extraordinary refractive index

$$n(z) = \frac{\epsilon_{\parallel}^{1/2} \epsilon_{\perp}^{1/2}}{(\epsilon_{\parallel} \cos^2 \theta + \epsilon_{\perp} \sin^2 \theta)^{1/2}}. \quad (6)$$

The overall phase shift induced by the optical field across the film is then given by

$$\phi = \frac{2\pi}{\lambda} \int_0^d n(z) - \epsilon_{\perp}^{1/2} dz. \quad (7)$$

Figure 2 shows the calculated ϕ versus I induced in a 250 μm homeotropic 4-cyano-4-pentylbiphenyl (5CB) film at three different incident angles. The theoretical curves are in good agreement with the experimental result. We noticed that in the $\alpha = 0$ case, reorientation occurs only when the pump beam intensity is above a threshold value. Analogous to the dc-field-induced reorientation, such a critical behavior is known as the Freedericksz transition. As seen in Fig. 2, near Freedericksz transition a small change in the pump intensity I can induce a rather appreciable change in the phase shift. One can use a bias field, which can be either optical or dc, to selectively place the initial operating point on the characteristic curve

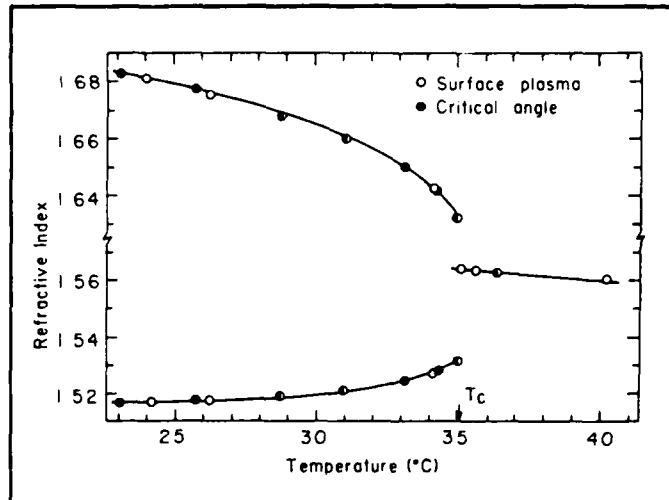


Fig. 3. Refractive indices of 5CB versus temperature, measured by the surface plasmon technique (open circles) and by the critical angle method (solid circles). (After Ref. 39.)

(ϕ versus I). If the operating point on the $\alpha = 0$ curve is set near the transition threshold in Fig. 2, then a pump intensity of a few W/cm^2 is already sufficient to induce a π phase shift. Such an intensity is obtainable even with a focused He-Ne laser beam. The average value of the induced refractive index change across the film in this case is $\Delta n \sim 10^{-3}$, or $\Delta n/|E|^2 \sim 2 \times 10^{-2}$ esu, which is 2×10^9 times larger than for CS_2 .

As one would expect, the very large Δn is generally associated with a very slow response. The dynamic response of director reorientation is quite complex. With some simplifying assumptions, it can be shown that the induced phase shift obeys the following relaxation equation³³:

$$\left(\frac{\partial}{\partial \tau} + \frac{1}{\tau_{\theta}} \right) \phi = \frac{\alpha_{\theta}}{\tau_{\theta}} I, \quad (8)$$

where α_{θ} is a constant depending on the initial orientation of the director and $\tau_{\theta} \approx \gamma/[\pi^2 K/d^2 - G]$ is the relaxation time, where γ is a viscosity coefficient and G is a function of the bias field. Both theory and experiment show that τ_{θ} is of the order of a few seconds to a few tenths of a second for a 5CB film of $\sim 100 \mu\text{m}$. Taking the average $\Delta n/|E|^2$ to be $\sim 2 \times 10^{-2}$ esu, we have a figure of merit $\beta \approx \Delta n/(|E|^2 \tau_{\theta}) \approx 2 \times 10^{-3}$ esu/s, which is about the same as that for 5CB in the isotropic phase. In comparison, β is ~ 5 esu/s for CS_2 . Thus, in some applications, if both the speed and the magnitude of the nonlinear optical response are important, then nematic liquid crystals are certainly not the best materials to be used in spite of their very high $\Delta n/|E|^2$.

Director reorientation by optical fields can in principle also occur in smectic and cholesteric liquid crystals. The situation is, however, much more complicated because of additional constraints arising from the ordered structures characteristic of such phases. Although theoretical calculations predict the possibility of observing director reorientation in these materials,³⁴⁻³⁷ thorough experimental studies of the effect have not yet been carried out.

Aside from laser-induced molecular reorientations, laser heating can also induce a change in the refractive index of the liquid crystal.³⁸ Even in normally transparent liquid crystalline materials, residual adsorption of a laser beam can lead to a detectable temperature rise. For example, propagation of a 350 W/cm^2 cw Ar^+ laser beam through a 100 μm 5CB film results in a temperature rise of ~ 2 K on the beam axis. The refractive index change due to heating is

given by

$$\Delta n = \frac{\delta n}{\delta T} \Delta T \quad (9)$$

In the isotropic phase, $\delta n / \delta T$ is not very different from those of other organic liquids and is generally dominated by thermal expansion. Typically, $\delta n / \delta T$ is of the order of $5 \times 10^{-4} \text{ K}^{-1}$. In the mesophases, the temperature rises also affect the degree of molecular alignment and hence the refractive indices. Similar to Eq. (1), we can define the order parameter Q of a nematic liquid crystal by the relations

$$\begin{aligned} n_{xx} &= \bar{n} + \frac{2}{3} \Delta n_0 Q \\ n_{yy} &= n_{zz} = \bar{n} - \frac{1}{3} \Delta n_0 Q \end{aligned} \quad (10)$$

We then have

$$\begin{aligned} \frac{\partial n_{xx}}{\partial T} &= \frac{\partial \bar{n}}{\partial T} + \frac{2}{3} Q \frac{\partial \Delta n_0}{\partial T} + \frac{2}{3} \Delta n_0 \frac{\partial Q}{\partial T} \\ &= \frac{\partial \bar{n}}{\partial T} + \frac{2}{3} \Delta n_0 \frac{\partial Q}{\partial T} \end{aligned} \quad (11)$$

$$\frac{\partial n_{xx}}{\partial T} - \frac{\partial n_{yy}}{\partial T} = \Delta n_0 \frac{\partial Q}{\partial T}$$

Figure 3 shows, as an example, how n_{xx} and n_{yy} of 5CB vary with temperature.³⁹ In the nematic phase, the term $\Delta n_0 (\partial Q / \partial T)$ is of the same order of magnitude as $\partial \bar{n} / \partial T$, which is nearly the same as that in the isotropic phase.

The dynamics of the laser-induced thermal effect are also very complex. With simplifying approximations, the induced phase shift ϕ_T across a film can be described by a thermal relaxation equation driven by laser heating³³:

$$\left(\frac{\partial}{\partial t} + \frac{1}{\tau_T} \right) \phi_T = - \frac{\alpha_T}{\tau_T} I \quad (12)$$

where α_T is proportional to the absorption coefficient, $\tau_T \sim d^2 / \pi^2 D$ is the relaxation time, and D is the heat diffusion constant. For a 100 μm film, τ_T is of the order of 0.1 s, which could be two or three orders of magnitude shorter than the orientational relaxation time τ_θ . If we take $\Delta n / |E|^2 \sim 10^{-3} \text{ esu}$ and $\tau_T \sim 0.1 \text{ s}$ for the laser-induced thermal effect, the corresponding figure of merit $\beta = \Delta n / |E|^2 \tau_T$ is $\sim 10^{-2} \text{ esu/s}$. Both laser-induced molecular reorientation and laser-induced thermal effect may influence the observed nonlinear optical effects in liquid crystals, as will be shown in the following sections.

3. NONLINEAR OPTICAL EFFECTS IN LIQUID CRYSTALS

Nonlinear optical effects in liquid crystals are readily observable. Because of the difference in the magnitudes of optical nonlinearities, studies of nonlinear optical processes in the isotropic phase generally require fairly high-power pulsed lasers. On the other hand, for observation of nonlinear optical effects in mesophases, a medium-power cw laser beam would suffice. Here, we briefly describe a variety of nonlinear optical processes in liquid crystals that have been studied quite extensively in the past and also some of the newly observed interesting phenomena.

3.1. Harmonic generation

Bulk liquid crystals are centrosymmetric. Second harmonic generation is allowed only if a dc field is employed to break the centro-

symmetry. Phase matching can be achieved by proper choice of the polarization and wave vector of the fundamental beam with respect to the director axis. The observed nonlinearity is comparable to that observed in CS_2 . Saha and Wong⁴⁰ have shown that the process could be used to study nematic ordering. They pointed out that smectic liquid crystals, because of their relatively lower scattering loss and the possibility of fabricating large crystals, could be developed into useful harmonic generators, but experimental demonstrations remain to be seen.

Third harmonic generation has been observed in cholesteric liquid crystals.⁴¹⁻⁴⁴ In this case, phase matching can be achieved via the Umklapp process with the help of the helical structure in cholesteric liquid crystals, as demonstrated by Shelton and Shen. Experimental results agree very well with the theory based on the continuous model proposed by deVries.⁴⁴

3.2. Degenerate wave mixing and phase conjugation

There have been extensive studies of degenerate wave mixing in liquid crystals. The process involves the formation of a refractive index grating in the medium by input laser beams, followed by diffraction of the input beams by the grating. As is well known, phase conjugation is just a special case of degenerate four-wave mixing.

Fekete et al. have successfully employed isotropic liquid crystals for phase conjugation.⁴⁵ As was discussed in Sec. 2, liquid crystals in the nematic phase have much larger optical-field-induced refractive index changes than in the isotropic phase. Degenerate wave mixing and phase conjugation can therefore be observed even with low power cw laser beams.^{17,19}

Multiple-order diffraction shows up when the laser intensities are of the order of tens of W/cm^2 . If the values of the optical-field-induced refractive index changes are known, the diffraction pattern and efficiency in the thin-film case can be quantitatively described by a simple theory of induced phase modulation on the incoming beams.

It is possible to use beams at one frequency to induce a refractive index grating, which subsequently diffracts an incoming beam at another frequency. This has been demonstrated with Nd:YAG and He-Ne lasers in a nematic film. The process could find practical applications in infrared-to-visible image conversions.^{46,47}

Phase conjugation (or wavefront reconstruction) using liquid crystals often suffers from speckle noise associated with a coherent beam [Fig. 4(a)]. This can be eliminated⁴⁸ if the input beams in the process are made partially incoherent by passing the laser beam through, for example, a rotating ground glass. A typical conjugated beam is shown in Fig. 4(b). The absence of the background speckle noise is also evident from the photo of the partially incoherent beam distorted by the phase aberrator [Fig. 4(c)]. The idea here is to impart sufficient incoherence to the background noise while retaining sufficient coherence for wavefront reconstruction.

3.3. Self-focusing and self-phase modulation

A laser beam with a transverse intensity profile should induce a spatially varying refractive index, which could lead to a spatial self-phase modulation on the beam and possibly to self-focusing of the beam. Similarly, the time variation of a pulsed laser beam could also lead to a time-varying phase modulation on the beam itself.

The study of self-focusing in liquid crystals dates back to the early 1970s, when the self-focusing phenomenon itself was under intensive investigation. In particular, transient self-focusing was difficult to understand. It turns out that the induced refractive index in an isotropic liquid crystal has a response time that can be varied by temperature over a wide range (a few ns to 1 μs) because of the critical slowing-down behavior. Consequently, such a medium is ideal for the study of transient self-focusing. Typically, the experiment uses a laser intensity on the order of 10^2 MW/cm^2 and a beam propagation length of about 10 cm in the medium. In traversing the medium, both the laser intensity and the phase undergo severe distortion.

Self-focusing also occurs in nematic liquid crystal films, but the situation is very different. The typical film thickness is $\sim 100 \mu\text{m}$; even so, because of the extremely large nonlinearity in the nematic

enough for the observation. Two different schemes¹⁸⁻²¹ have been used to achieve optical bistability. One is the usual nonlinear Fabry-Perot interferometer with an intracavity nematic film; the other utilizes self-focusing with an external feedback.

In the nonlinear Fabry-Perot interferometer of Khoo et al.,¹⁹⁻²¹ a 50 μm homeotropic sample tilted at 45° in a 4 cm long cavity was used. Bistability was observed with an Ar⁺ laser at an input intensity of about 600 W/cm². Formation of spatial rings and oscillatory behavior in the output were observed at high input intensity. Cheung et al.¹⁸ took a much shorter cavity formed by a 83 μm film sandwiched between two mirrors. A magnetic field was used to move the operation point above the Freedericksz transition in the film (see Sec. 2) in order to increase the optical nonlinearity. As a result, a much smaller laser intensity was needed for bistable switching (~ 10 W/cm²). At higher input intensities, the output broke up into periodic oscillations. This was found to be due to the interplay between the laser-induced reorientation, which contributes to a positive phase shift with a slower response time, and laser heating, which contributes to a negative phase shift with a faster response time. The experimental results were shown to agree well with the theoretical calculation. The same reason probably also explains the oscillatory behavior observed by Khoo et al.

Study of optical bistability resulting from self-focusing with external feedback is a relatively recent endeavor. The experimental situation is schematically depicted in Fig. 7(a). A laser beam with a certain prescribed wavefront is incident on the nematic film, and the transmitted beam is partially reflected onto the film by a mirror to create a feedback in the field-induced refractive index in the film. The variation of the output through a pinhole behind the mirror with the input laser power exhibits optical bistability.

A detailed theory for such a cavityless optical bistability proposed earlier by Kaplan⁴⁹ has been worked out.^{50,51} Essentially, with a proper arrangement of the lens, mirrors, and the wavefront of the input beam, the feedback can reinforce the self-phase modulation effect, leading to bistability. Figures 7(b) and 7(c) show some examples of the observed bistability curves, with the pinhole at the on-axis and the off-axis locations, respectively.

4. CONCLUSION

We have presented a brief summary of the basic nonlinear optical properties of liquid crystals and some observed nonlinear optical processes in liquid crystals. The unique physical and optical characteristics of liquid crystals open up some exciting areas of research that are of fundamental as well as applied interest. There are a number of other experiments in this field that we have not discussed here. Recently, Hsiung et al.³³ have used nanosecond laser pulses to study the dynamics of molecular reorientation as well as the laser-induced thermal effect in a nematic film. Khoo and Normandin have observed the generation of ultrahigh frequency acoustic waves and their effects on the laser-induced thermal gratings by nanosecond laser pulses in nematic⁵⁵ as well as smectic liquid crystals.⁵⁶ Optical switching at a nonlinear interface formed by nematic liquid crystals and glass^{57,58} and nonlinear optical propagation in a planar waveguide cladded by liquid crystals⁵⁹ have also been observed. Although there are physical limitations to the use of liquid crystals in optical devices (the most serious of which is the response time), nonlinear optical studies in liquid crystals have continuously provided us with some new insights into the basic understanding of optical phenomena in a nonlinear medium and also into the potential applications of such materials.

5. ACKNOWLEDGMENTS

I. C. Khoo acknowledges the support of the National Science Foundation (ECS8415387) and the Air Force Office of Scientific Research (AFOSR840375). Y. R. Shen's research is supported by a National Science Foundation grant (DMR81-17366).

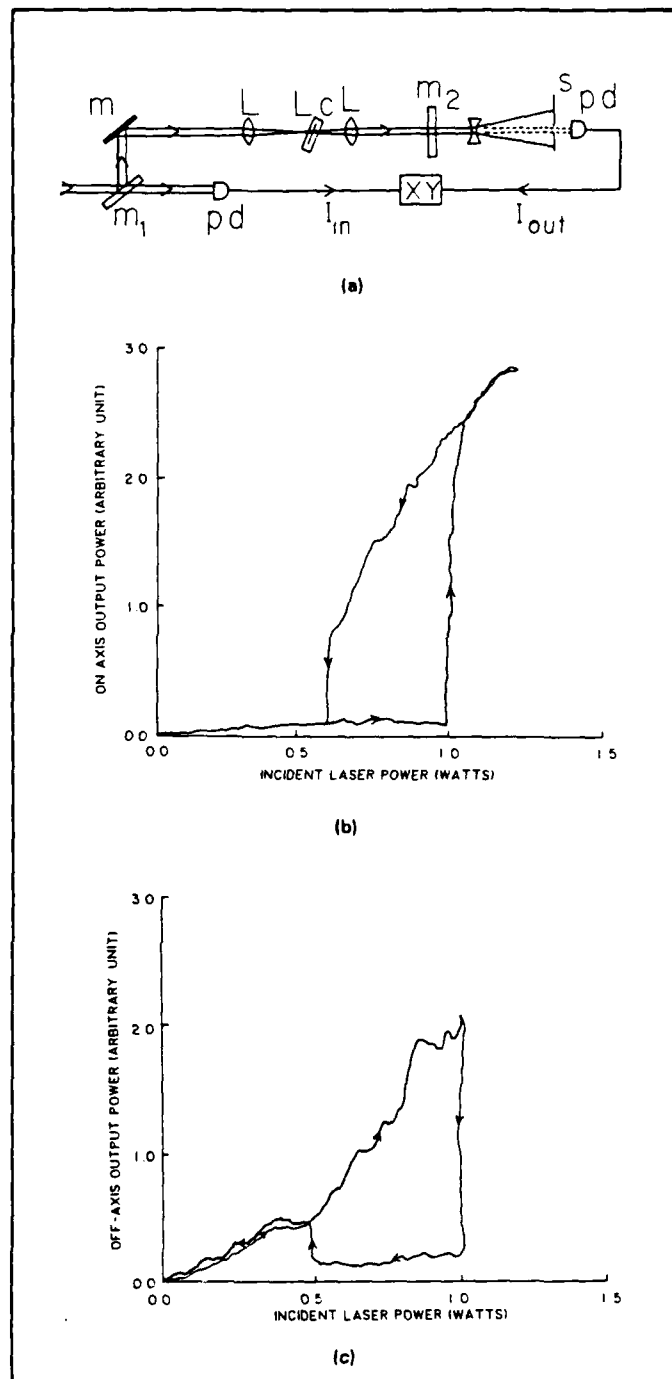


Fig. 7. (a) Experimental setup for observation of transverse intensity bistability. (b) Experimentally observed bistability of the power in the central region of the transmitted beam. (c) Experimentally observed bistability of the power in the off-axis region of the transmitted beam. (After Ref. 51.)

6. REFERENCES

- See, for example, E. B. Priestley, P. J. Wojtowicz, and P. Sheng, *Introduction to Liquid Crystals*, Plenum Press, New York (1975).
- See, for example, P. deGennes, *The Physics of Liquid Crystals*, Oxford University Press, Oxford (1974).
- See, for example, *Liquid Crystal Devices*, T. Kallard, ed., Optosonic Press, New York (1973).
- See, for example, M. Tobias, *International Handbook of Liquid Crystal Displays*, Ovum Ltd., London (1975).

5. Y. R. Shen, in *Nonlinear Spectroscopy*, N. Bloembergen, ed., Proc. Int. School of Physics, "Enrico Fermi," Course 64 pp. 201-216, North Holland Publishing Co., Amsterdam (1977).
6. R. M. Herman and R. J. Serinko, *Phys. Rev.* A19, 1757 (1979).
7. G. K. L. Wong and Y. R. Shen, *Phys. Rev. Lett.* 32, 527 (1974).
8. D. V. G. L. N. Rao and S. Jayaraman, *Appl. Phys. Lett.* 23, 539 (1973).
9. E. G. Hanson, G. K. L. Wong, and Y. R. Shen, *Opt. Comun.* 20, 45 (1977).
10. I. C. Khoo, S. L. Zhuang, and S. Shepard, *Appl. Phys. Lett.* 39, 937 (1981).
11. S. D. Durbin, S. M. Arakelian, and Y. R. Shen, *Opt. Lett.* 6, 411 (1981).
12. N. F. Pilipetski, A. V. Sukhov, N. V. Tabiryan, and B. Ya Zel'dovich, *Opt. Commun.* 37, 280 (1981).
13. S. D. Durbin, S. M. Arakelian, and Y. R. Shen, *Opt. Lett.* 7, 145 (1982).
14. I. C. Khoo, *Appl. Phys. Lett.* 38, 123 (1981).
15. I. C. Khoo and S. L. Zhuang, *Appl. Phys. Lett.* 37, 3 (1980).
16. I. C. Khoo, *Phys. Rev.* A25, 1040 (1982).
17. I. C. Khoo and S. L. Zhuang, *IEEE J. Quantum Electron.* QE-18, 246 (1982).
18. M. M. Cheung, S. D. Durbin, and Y. R. Shen, *Opt. Lett.* 8, 39 (1983).
19. I. C. Khoo, *Appl. Phys. Lett.* 41, 909 (1982).
20. I. C. Khoo, J. Y. Hou, R. Normandin, and V. C. Y. So, *Phys. Rev.* A27, 3251 (1983).
21. I. C. Khoo, J. Y. Hou, R. Normandin, and V. C. Y. So, *J. Appl. Phys.* 53, 7599 (1982).
22. G. K. L. Wong and Y. R. Shen, *Phys. Rev. Lett.* 30, 895 (1973).
23. G. K. L. Wong and Y. R. Shen, *Phys. Rev.* A10, 1277 (1974).
24. B. Y. Zel'dovich, N. F. Pelipetskii, A. V. Sukhov, and N. V. Tabiryan, *JETP Lett.* 31, 263 (1980).
25. A. S. Zolot'ko, V. F. Kataeva, N. Kroo, N. N. Sobolev, and L. Csillag, *JETP Lett.* 32, 158 (1980).
26. I. C. Khoo and S. L. Zhuang, *Appl. Phys. Lett.* 37, 3 (1980).
27. I. C. Khoo, *Phys. Rev.* A23, 2077 (1981).
28. I. C. Khoo, *Phys. Rev.* A25, 1636 (1982).
29. I. C. Khoo, *Phys. Rev.* A27, 2747 (1983).
30. S. D. Durbin, S. M. Arakelian, and Y. R. Shen, *Phys. Rev. Lett.* 47, 1411 (1981).
31. H. L. Ong, *Phys. Rev.* A28, 2393 (1983).
32. S. D. Durbin, Ph.D. Thesis, Univ. of California, Berkeley (1984) (unpublished).
33. H. Hsiung, L. P. Shi, and Y. R. Shen, *Phys. Rev.* A30, 1453 (1984).
34. N. V. Tabiryan and B. Ya. Zel'dovich, *Mol. Cryst. Liq. Cryst.* 69, 19 (1981).
35. N. V. Tabiryan and B. Ya. Zel'dovich, *Mol. Cryst. Liq. Cryst.* 69, 31 (1981).
36. H. G. Winful, *Phys. Rev. Lett.* 49, 1179 (1982).
37. H. L. Ong and C. Y. Young, *Phys. Rev.* A29, 297 (1984).
38. I. C. Khoo and R. Normandin, *IEEE J. Quantum Electron.* (1985).
39. K. C. Chu, C. K. Chen, and Y. R. Shen, *Mol. Cryst. Liq. Cryst.* 59, 97 (1980).
40. S. K. Saha and G. K. Wong, *Appl. Phys. Lett.* 34, 423 (1979).
41. J. W. Shelton and Y. R. Shen, *Phys. Rev. Lett.* 25, 23 (1970).
42. J. W. Shelton and Y. R. Shen, *Phys. Rev. Lett.* 26, 538 (1971).
43. J. W. Shelton and Y. R. Shen, *Phys. Rev.* A5, 1867 (1972).
44. H. N. deVries, *Acta Cryst.* 4, 219 (1951).
45. D. Fekete, J. AuYeung, and A. Yariv, *Opt. Lett.* 5, 51 (1979).
46. G. Martin and R. W. Hellwarth, *Appl. Phys. Lett.* 34, 371 (1979).
47. I. C. Khoo and R. Normandin, to be published in *Technical Digest, Conf. on Lasers and Electro-Optics '85*.
48. E. Leith, H. Chen, Y. Cheng, G. Swanson, and I. C. Khoo, *Proc. 5th Rochester Conf. on Coherence and Quantum Optics, Rochester, N.Y.* (1983).
49. A. E. Kaplan, *Opt. Lett.* 6, 360 (1981).
50. I. C. Khoo, *Appl. Phys. Lett.* 41, 909 (1982).
51. I. C. Khoo, T. H. Liu, P. Y. Yan, S. Shepard, and J. Y. Hou, *Phys. Rev.* A29, 2756 (1984).
52. I. C. Khoo, T. H. Liu, and R. Normandin, to be published in *Mol. Cryst. Liq. Cryst.*
53. T. Bischoffberger and Y. R. Shen, *Appl. Phys. Lett.* 28, 731 (1976).
54. T. Bischoffberger and Y. R. Shen, *Phys. Rev.* A17, 335 (1978).
55. I. C. Khoo and R. Normandin, *Opt. Lett.* 9, 285 (1984).
56. I. C. Khoo and R. Normandin, *J. Appl. Phys.* 55, 1416 (1984).
57. I. C. Khoo, *Appl. Phys. Lett.* 40, 645 (1982).
58. I. C. Khoo and J. Y. Hou, *J. Opt. Soc. Am. B.* (May 1985).
59. H. Vach, C. T. Seaton, G. I. Stegeman, and I. C. Khoo, *Opt. Lett.* 9, 238 (1984).

The Mechanism and Dynamics of Transient Thermal Grating Diffraction in Nematic Liquid Crystal Films

IAM-CHOON KHOO, MEMBER, IEEE, AND RICHARD NORMANDIN

Abstract—We have studied the mechanism and the dynamics of degenerate four-wave mixing in a nematic liquid crystal film. Nanosecond laser pulses are used to generate an index grating associated with the changes in the density and in the order parameter. We have measured and analyzed the contributions from these two mechanisms, their interference effects rise and decay time constants, and have also performed a detailed analysis of the diffraction efficiency. This study quantitatively characterizes the potential usefulness of nematic films for four-wave mixing based applications.

INTRODUCTION

RECENT studies have demonstrated extraordinarily large optical nonlinearity of nematic liquid crystal arising from the optically induced reorientation of the molecular director axis [1]–[3]. The nonlinearity has been shown to be several orders of magnitude larger than that exhibited by a typical anisotropic liquid like CS_2 and is in the same order of magnitude as those observed in some nonlinear photorefractive crystals (e.g., BaTiO_4) or semiconductors. The response time of molecular reorientation in nematics is dependent on the optical intensity, ranging from seconds (optical intensity $\approx \text{W/cm}^2$) to microsecond or less (optical intensity $\approx \text{MW/cm}^2$), among other factors. Wavefront conjugation [4], optical bistability [5], and other optical processes [6] have been demonstrated using CW low-power lasers. In some nematic liquid crystals, e.g., MBBA (p-methoxybenzylidene-p-n-butylaniline), an equally large thermal indexing effect [1], [7] has been observed, due to the crystal's natural absorption and unusually high thermal index gradient dn/dT (where n denotes the refractive index and T the temperature). Laser induced thermal refractive index change in liquid crystalline media is a well-known effect, and has been studied in many other contexts [8]. Recently, thermal grating has received considerable attention in the study of degenerate four-wave mixing as a useful mechanism for high-power wavefront conjugation [9], [10]. Martin and Hellwarth, for example, have studied a wide variety of liquids with dissolved dyes in infrared-to-visible image conversion processes. Others have shown amplified reflections and high fidelity phase aberration corrected imaging results [11], [12].

In this paper, we present detailed experimental results and

Manuscript received September 5, 1984; revised November 15, 1984. This work was supported in part by the National Science Foundation under Grant ECS8415387 and by the Air Force Office of Scientific Research under Grant AFOSR 840375.

I.-C. Khoo is with the Department of Electrical Engineering, The Pennsylvania State University, University Park, PA 16802.

R. Normandin is with the Division of Microstructural Sciences, the National Research Council of Canada, Ottawa, Ont., Canada K1A 0R6.

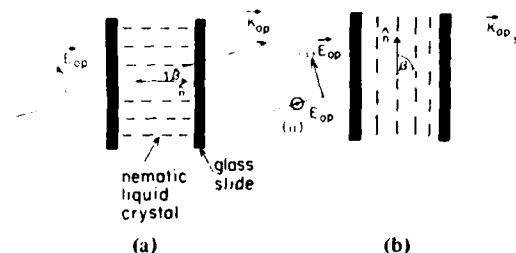


Fig. 1. Schematics of the laser-nematic interaction in two typical nematic cells. (a) Homeotropically aligned nematics. (b) Planar nematic cell. Case (i) is for extraordinary ray. Case (ii) for ordinary ray (\vec{E}_{op} is orthogonal to the nematic director axis).

analysis of the basic mechanism for thermal indexing effects in nematic liquid crystals, whose refractive index in the nematic phase depends on the density ρ (as in liquid and crystals) and the order parameter S (unique for the liquid crystal phase). Degenerate four-wave mixing experiments are carried out with nanosecond laser pulses, and results for various parameters such as the diffraction efficiencies, the grating decay and on-set time, acoustic contribution, etc., are obtained. In the next section we will review the relevant theory of nematogen and some quantitative expressions for the laser induced density and order parameter gratings, and the roles played by various nematic, geometrical, and optical parameters. This is followed by detailed experimental results and an analysis.

THEORETICAL CONSIDERATIONS

Under excitation by nanosecond laser pulses, the thermal indexing effect in nematic is due to some finite absorption by the nematic at the wavelength of the laser. The absorption rate varies from material to material, and may often be aided by some dissolved dyes. It is perhaps more illuminating if we limit our attention to some exemplary geometries of interaction between the polarization of the laser and the director axis of the nematic, for two commonly occurring nematic cell alignments (planar and homeotropic). As depicted in Fig. 1(a) and (b), the optical propagation makes an angle β with respect to the nematic director axis \vec{n} . In Fig. 1(a), the beam propagates as an extraordinary ray with a refractive index n_e given by [13]

$$n_e = \frac{n_1 n_{||}}{(n_{||}^2 \cos^2 \beta + n_1^2 \sin^2 \beta)^{1/2}} \quad (1)$$

For Fig. 1(b), the beam propagates as an extraordinary ray in case (i), and as an ordinary ray with the refractive index n_1 in case (ii).

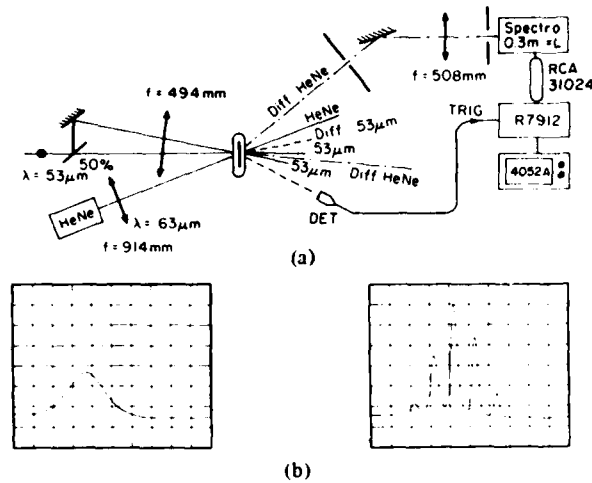


Fig. 2. Schematics of the experimental setup. \odot is the wave-mixing in air. (\odot in liquid crystal is $2/3$ of \odot in air). The incident Nd:YAG SHG pulses and the He-Ne lasers are all in the same plane. (a) A single mode pump laser pulse. (b) A modulated two-mode pump laser pulse. Intensity profile as a function of time. Time scale: 10 ns/div.

Depending on the laser wavelength and intensity, the optically induced refractive index change originates from molecular reorientation and/or thermal heating. Pulsed laser induced molecular reorientation can occur in the configurations depicted in Fig. 1(a) and (b) [case (i)] [14], [15]. The basic mechanism is similar to that observed using a CW laser, with a rise time that depends on the laser intensity. Typically, one can estimate using well-known nematic theory that an optical intensity on the order of 100 MW/cm^2 is needed to see significant reorientation in the nanosecond time scale. Under this intensity, the accompanying thermal index effect is very large and tends to mask the reorientational effect. There is also a practical consideration not to involve the molecular reorientation, which is characterized by a very slow recovery time (typically about 1 s for a $40 \mu\text{m}$ thick sample).

For incident optical fields at $\beta = 0$, two distinct thermal index changes are induced Δn_{\parallel} and Δn_{\perp} , corresponding to case (i) and case (ii), respectively. We shall henceforth limit our discussion to the planar sample depicted in Fig. 1(b). Similar results have been obtained for the homeotropic sample [Fig. 1(a)], where the thermal index gradient involved is dn_{\perp}/dT .

We are interested in a degenerate four-wave mixing configuration. As depicted in Fig. 2, the applied optical field consists of two lasers intersecting at a wave mixing angle θ in the xy plane and incident at an angle $\beta = 0$ on a planar sample with the polarization parallel to or perpendicular to the director axis. We have used wave mixing angles ranging from 1 to 12° , corresponding to optical grating constant ranging between about $34 \mu\text{m}$ (1°) to about $5 \mu\text{m}$. The grating is characterized by a wave vector \vec{q} ($\vec{q} = \vec{k}_1 - \vec{k}_2$). In case (i), \vec{q} is almost normal to n while in case (ii), \vec{q} is almost parallel to n . Obviously, for a finite wave mixing angle, the grating wave vector \vec{q} is not exactly normal (or parallel) to n . However, since the wave mixing angle is small, the correction factor for components in the directions other than the ones stated is small and may be neglected.

Following standard nematic theory, the optical dielectric

constants $\epsilon_{\parallel}(n_{\parallel}^2)$ and $\epsilon_{\perp}(n_{\perp}^2)$ are given by

$$\epsilon_{\parallel} = \epsilon_l(T) + 2/3 \Delta\epsilon(T) \quad (2)$$

and

$$\epsilon_{\perp} = \epsilon_l(T) - 1/3 \Delta\epsilon(T) \quad (3)$$

where $\epsilon_l(T)$ is the dielectric constant associated with the nematic in the zero-ordered phase ($S = 0$)

$$\epsilon_l = 1 + \frac{N\rho}{3\epsilon_0 M} (\alpha_l k_l + 2\alpha_T k_T); \quad \epsilon_l \sim 1 + \text{const. } \rho. \quad (4)$$

ρ is the density of the nematic and $\alpha_{l,T}$ and $k_{l,T}$ are the longitudinal and transverse components of the molecular electronic polarization tensor α and the internal field tensor $K^{2,3}$. The dielectric anisotropy $\Delta\epsilon$ is given by

$$\Delta\epsilon = \frac{N\rho}{\epsilon_0 M} (\alpha_l k_l - \alpha_T k_T); \quad \Delta\epsilon \sim \rho S \quad (5)$$

where S is the order parameter. The order parameter in most nematics is well approximated by the expression.

$$S = \left(1 - 0.98 \frac{TV^2}{T_{Ni} V_{Ni}^2} \right)^{0.22} \quad (6)$$

where T_{Ni} is the nematic \leftrightarrow isotropic phase transition temperature, and V 's are the corresponding molar volumes. In general, therefore, the dielectric constant ϵ of a particular nematic is a function of ρ and S , which in turn depend on T .

Studies of thermal index change in nematics can be extremely complicated, since almost all the parameters mentioned so far (ρ , S , V), and other parameters (e.g., specific heat) that are important in wave mixing diffraction efficiency are temperature dependent. It is futile and probably meaningless to account for all temperature dependences. We shall focus here on the induced density and order parameters changes, whose effects dominate the wave mixing processes.

Equations (4) and (5) can be rewritten to give

$$\epsilon_l = 1 + C_1 \rho \quad (4a)$$

and

$$\Delta\epsilon = C_2 \rho S \quad (5a)$$

where C_1 and C_2 are constants deducible from (4) and (5). From known values of ρ ($\sim 1 \text{ gm} \cdot \text{cm}^{-3}$), $S(0.6)$, $\Delta\epsilon(0.65)$, and $\epsilon_l((1.53)^2)$ for PCB (at 20°C), we get $C_1 \sim 1.33$ and $C_2 \sim 1.12$, combining (4) and (5) and using $n^2 = \epsilon$, we get

$$\frac{dn_{\perp}}{dT} = 2n^{-1} \left[(1.33 - 0.37S) \frac{d\rho}{dT} - 0.37 \frac{dS}{dT} \right]. \quad (7)$$

For PCB, S ranges from about 0.6 (at 20°C) to near vanishing value at T_{Ni} . Notice that for dn_{\parallel}/dT , we get a similar expression as (7) with the numerical factor (-0.37) on the right-hand side replaced by (0.74). Both $d\rho/dT$ and dS/dT are negative. However, dS/dT is larger in magnitude and therefore dn_{\parallel}/dT is negative and dn_{\perp}/dT is positive.

Some numerical estimates may be illustrative. Consider PCB at 20°C . Using measured values of $d\rho/dT$ ($6 \times 10^{-4} \text{ gm/cm}^{-3}$

K^{-1}), ρ (1 gm/cm^{-3}), and the value of 0.37 dS/dT calculated from (6) ($-6.9 \times 10^{-3} \text{ K}^{-1}$), we get $dn/dT \sim (-2.7 \times 10^{-4} + 6.9 \times 10^{-4}) \sim 4.2 \times 10^{-4} \text{ K}^{-1}$. This value agrees with the experimental value of 4×10^{-4} quite closely. Fig. 3 shows experimental values of $dn_{||}/dT$ and dn_{\perp}/dT and some theoretical points. Values calculated for other temperatures also agrees fairly with experimental results, although discrepancies arise as one approaches T_{Ni} . There are several reasons for the discrepancies. One possibly is due to the breakdown of the mean field theory on which the expressions for S and ϵ are based. Secondly, we have not included any near-field corrections in our calculation. Nevertheless, the point to note from these plots is the largeness of dn/dT and its dramatic increase with temperature.

Following a short laser pulse, a temperature grating $\Delta T(\vec{q}; t)$ is generated in the medium. The response of the medium as observed in our experiment follows the time-integrated intensity of the laser, and maximum diffraction is observed immediately following (within the laser pulsewidth) the laser. The resultant refractive index grating $\Delta n(\vec{q}; t)$ consists of two components. One is associated with the order parameter fluctuations $\Delta S(\vec{q}; t)$ while the other with the density fluctuation $\Delta \rho(\vec{q}; t)$. Under appropriate conditions (e.g., comparable magnitude of contribution in Δn from ΔS and $\Delta \rho$) the propagating $\Delta \rho$ grating will interfere with the nonpropagating (diffusive type) ΔS grating, leading to modulation in the diffraction from the grating [16], [17]. The period of modulation f_S^{-1} of the temporal behavior of the diffraction from the grating (of a CW probe laser) is simply given by $2\pi/|\vec{q}| C_s^{-1}$ (where C_s is the velocity of sound and $|\vec{q}| = 2|\vec{k}| \sin \theta/2$).

For a quantitative analysis of the diffraction efficiency, we note here an important point with respect to nematics, namely, that the thermal index gradient dn/dT is not a constant as a function of the temperature. As a matter of fact, it increases by more than one order of magnitude as one approaches the nematic \leftrightarrow isotropic phase transition [18] (cf., Fig. 3). Furthermore, values of the ρ , the heat capacity C_p , and the absorption coefficient α of the material needed for calculating the diffraction efficiency, are also sensitive to the temperature [19]. To get a good (and semiquantitative) insight into the diffraction efficiency, we choose for our theoretical calculations the parameters ΔT (rise in temperature), and Δn (the corresponding change in the refractive index), associated with the input pump energies. Both parameters can be easily measured experimentally. In the language of the usual four-wave mixing calculations [20], the two pump lasers set up an index grating Δn that oscillates spatially with a wave vector $\vec{q} = \vec{k}_1 - \vec{k}_2$. In conjunction with a probe laser (incident at \vec{k}_1 , say), this generates a diffraction at $\vec{k}_4 = 2\vec{k}_1 - \vec{k}_2$. The maximum amplitude of the diffraction (corresponding to the maximum Δn , which, as a function of time, reaches a maximum value as the temperature of the sample rises to a maxima) is given by

$$E_D \cong \frac{k \Delta n E_1}{2n} \frac{(\sin \partial k d)}{\partial k} \quad (8)$$

assuming small absorption loss and small wave-mixing angles (valid in our case involving pure PCB). ∂k is the magnitude of

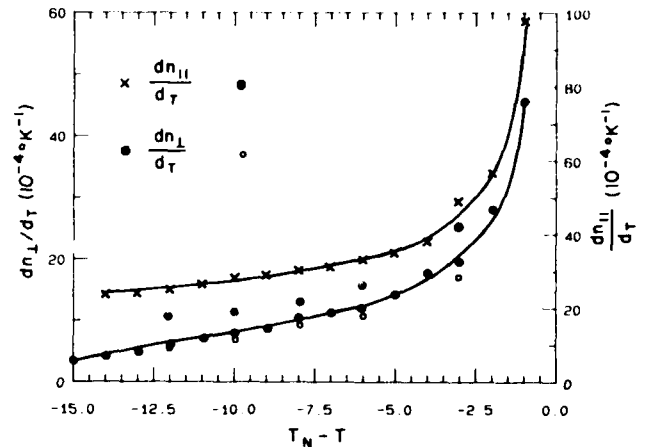


Fig. 3. Plot of $dn_{||}/dT$ and dn_{\perp}/dT for PCB as a function of temperature; data is deduced from [18]. Note that both dn/dT increase by an order of magnitude near T_{Ni} . The value of dn/dT of a high thermal index gradient liquid like cyclohexane is about $4 \times 10^{-4} \text{ K}^{-1}$. Some sample theoretical estimates are also indicated (\bullet and \circ).

the momentum mismatch. Equation (8) gives a maximum diffraction efficiency I_D/I_1 of

$$R_{\max} \sim \frac{k^2}{4n^2} (\Delta n)^2 \left(\frac{\sin \partial k d}{\partial k} \right)^2 \quad (9a)$$

For typical experimental parameters ($\lambda = 0.53 \text{ } \mu\text{m}$, $k_1 = k_2 = 2\pi/\lambda$, θ (in air) $= 2^\circ$, $d = 40 \text{ } \mu\text{m}$), $\partial k \sim k \theta^2 \sim (39 \text{ } \mu\text{m})^2$, which is close to $d^2 = (40 \text{ } \mu\text{m})^2$. Equation (9) possesses an obvious overestimate factor of the experimentally realizable diffraction efficiency. Both the probe and the diffracted beam suffer scattering loss in traversing the sample (typically about 20 percent due to reflections at the glass-air, glass-nematic boundaries, and the nematic orientational fluctuation scattering). These losses in conjunction also with the "Gaussian" shape intensity profiles of the beam can easily contribute to at least an order of magnitude lower diffraction efficiency in the actual observed value.

Alternatively, one can also use the thin phase grating expression as in [9], by replacing all the temperature dependent parameters like dn/dT , C_p , and ρ , by their average values. In the temperature range involved ($21\text{--}30^\circ\text{C}$), ρ and C_p varies only slightly (<10 percent), and thus can be assumed constant. On the other hand, dn/dT , (e.g., for $n_{||}$) changes by a factor of 2 (cf., Fig. 3), from ~ 0.0004 to ~ 0.001 . The average dn/dT is thus taken to be 0.0007. The only unknown parameter for PCB is the absorption coefficient α . This is estimated from experimental observation of the temperature rise for a given incident laser energy. We found that $\alpha d \sim 3 \times 10^{-3}$, where d is the sample thickness ($d \sim 40 \text{ } \mu\text{m}$). Following [9], the maximum diffraction efficiency is given

$$R_m \sim TD^2 U_1 U_2 \eta \quad (9b)$$

where T is the transmission coefficient at frequency ν of the third (probe) beam, $D = \nu \rho^{-1} C_p^{-1} dn/dT$, and U_1 and U_2 are the energies (per centimeter²) of the pump lasers, and $\eta \sim \alpha d$. We must remark here that both (9a) or (9b) are at best order of magnitude estimates of the diffraction efficiency.

The large change in the refractive index of liquid crystal over a small temperature rise is due to its inherently large thermal index. At 21° , dn_1/dT is $\sim 4 \times 10^{-4}$, which is already larger than almost all high index liquids [21] (e.g., CS_2 and cyclohexane). Note, however, that dn_{\parallel}/dT has an even larger magnitude $\sim 3 \times 10^{-3}$. Thus, utilizing Δn_{\parallel} (or Δn_{\perp} and Δn_{\parallel} near T_c , where both increase by an order of magnitude) will greatly enhance the diffraction efficiency.

EXPERIMENT

We have conducted experiments with principally two kinds of nematics: MBBA (p-methoxybenzylidene-p-n-butylaniline) and PCB (pentyl-cyano-biphenyl). PCB absorbs very little at the $0.53 \mu\text{m}$ (SHG of Nd:YAG) wavelength used. To increase the absorption, we have also used PCB samples with traces of dissolved dyes (Rhodamine 6G). Comparative studies are made for samples with dissolved dyes and the pure samples to ascertain the roles of the dye molecules. MBBA absorption at $0.53 \mu\text{m}$ is considerably more than PCB's. However, as often noted, MBBA is rather unstable with the age of the sample. The overall results obtained for MBBA are, however, similar to those obtained with PCB, which appears to be stable over a period of months.

The typical sample used is $40 \mu\text{m}$ thick. Planar alignment is obtained by the rubbing method with lens tissues. Sample temperature is maintained at 21° . (The nematic \leftrightarrow isotropic transition temperature T_c of PCB is 35° .) At this temperature, $n_{\perp} \sim 1.52$, $n_{\parallel} \sim 1.72$, and $n_{\text{liquid}} \sim 1.58$. The experimental setup is schematically depicted in Fig. 2. The pump laser pulses are derived from the SHG of a Q-switch Nd:YAG laser. The output from this laser is either in the single [Fig. 2(a)] or a time-modulated two-mode [Fig. 2(b)] state. The laser pulse width (FWHM) is typically 20 ns, and the laser energies used lie in the range of a few millijoules to 35 mj. The incident lasers are weakly focused at the sample to a spot size of $\sim 0.64 \text{ mm}^2$. The sample is oriented with the plane normal to the incident laser beams, with the director axis n oriented either parallel (\parallel) or perpendicular (\perp) to the optical field polarization. A linearly polarized He-Ne laser is used to probe the grating and the diffraction following each single pump laser shot is monitored with a monochromator-PMT setup and analyzed by a transient waveform digitizer or a fast storage scope.

RESULTS AND DISCUSSIONS

Depending on the wave-mixing angle and the type of pump-pulses used, there are essentially two types of time-dependence of the diffraction from the transient grating as probed by the He-Ne laser. Results quoted below involve the ordinary refractive index change Δn . One is depicted in Fig. 4(a), which is obtained using single-mode laser pulses [Fig. 2(a)]. We have a monotonic rise followed by a monotonic long-lived decay. The rise time is within the pulse length of the laser (which has a FWHM of about 20 ns). On the other hand, if the excitation is a time modulated [Fig. 2(b)] laser pulse, modulations due to the acoustic waves are observed during the first 100 ns or so of the diffraction, [as depicted in Fig. 4(b)] at an external wave-mixing angle $= 2^\circ$. At other angles, modulations are also

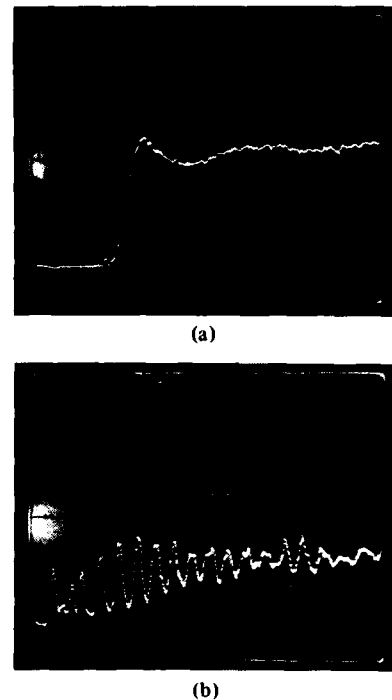


Fig. 4. The diffraction from the He-Ne as detected by the transient waveform digitizer. (a) Using single-mode Nd:YAG SHG as pump lasers. Time scale is 50 ns/dw, showing monotonic rise of the diffracted signal to a maximum within 50 ns from the start of the pump laser. (b) Modulated diffraction from the He-Ne. Time scale is 20 ns/dw.

observed but the modulation depth is less. The modulation is maximum at $\theta = 2^\circ$ because the modulation frequency is "at resonance" with the acoustic frequency as confirmed in a recent report [12]. Fig. 4(b) also allows us to estimate the acoustic attenuation time constant in nematic liquid crystal to be about 100 ns at the acoustic frequency of 90 MHz (since the interference effects between the density (acoustic) and the order parameter gratings decay in a time scale of this order). This is probably the first direct time-dependent measurement of the acoustic attenuation time constant. The velocity of sound inferred from these experimental measurements ($\sim 1.53 \times 10^5 \text{ cm/s}$) for nematic is in good agreement with known results.

More quantitative results of the density and order parameter can also be deduced from Fig. 4. The parameters used in the experiment for getting the results depicted in Fig. 4(b) are as follows. The energy in each of the pump beams is about 10 mj. The diffraction efficiency (associated with dn_1/dT) is measured to be 2 percent. The spot sizes of the incident laser beams are 0.6 mm^2 . The initial temperature of the sample is 21° . Pulse duration is about 20 ns (FWHM). In a separate experiment, we have estimated that the rise in the temperature of the sample is about 9°C . (To determine the temperature rise due to the laser pulses, we noted the total pulse energy needed to just heat the sample to the isotropic phase ($\approx 30 \text{ mj}$), i.e., 30 mj is needed to induce a 14° change in temperature. In our experiment, the total laser pulse energy is 20 mj, which gives us an estimate (by no means exact) of about 9° rise in temperature).

From known experimental data, this corresponds to a change in the refractive index Δn_{\perp} of 0.004. For the same tempera-

ture rise, the change in the refractive index $\Delta n_1(\rho)$ is -0.004 , implying therefore $\Delta n(S)$ associated with the order parameter of 0.0008 . Since $\Delta n_1(\rho)$ and $\Delta n_1(S)$ are comparable, one expects large modulations in the diffracted signal, which is indeed experimentally observed [cf., Fig. 4(b)]. In general, modulations are not detectable in samples where there is large induced temperature change (or refractive index change, equivalently) whence the $\Delta n(S)$ component dominates.

Using the experimental parameters ($\Delta n_1 = 0.004$, $d = 40 \mu\text{m}$, $\lambda = 0.53 \mu\text{m}$, $\theta_{\text{air}} = 2^\circ$), the forward diffracted efficiency as probed by the YAG laser pulses themselves can be estimated from (9a) to give $R_{\text{max}} \sim 2 \times 10^{-1}$. Using the expression (9b), with the parameters ($T \sim 1$), $D(\text{liquid crystal}) \sim 2 \times 10^{-2}$ (comparable to cyclohexane), $U_1 \sim U_2 \sim 1.6 \text{ J/cm}^2$, $\eta \sim 3 \times 10^{-3}$, we also get $R_{\text{max}} \sim 2 \times 10^{-1}$. Experimentally we observe a diffraction efficiency of 2×10^{-2} . There are several reasons for the experimentally observed lower diffraction efficiency. Principally, we have not included losses (in both the pump and the probe, as well as the signal) in the liquid crystals, from scattering and reflection losses from the glass slides. Secondly, the grating builds up on the order of the laser pulse duration, and thus probing it with a time coincident pulse of the same duration may well not give the highest efficiency estimated in the theory. Finally, beam spot size, nonuniform spatial intensity distributions, etc., that normally lower the experimentally observed value (compared to theory) are all expected to contribute to some errors.

It is not our intention here, of course, to delve into a detailed quantitative exposition of the diffraction efficiency. Rather, noting that the parameters governing the diffraction efficiency and their roles, one can draw some conclusions regarding means of optimizing the four-wave mixing process.

One obvious way is to employ dn_{\parallel}/dt (which is about seven times dn_{\perp}/dt in the same temperature range), as we will presently see. Another way is by going to a slightly thicker sample. Our previous experiments have indicated that $100 \mu\text{m}$ thick samples are probably ideal in terms of stability (alignment) and losses (scattering). These two factors could easily increase the diffractions by two orders of magnitude.

For the same temperature rise, the change in the extraordinary refractive index Δn_{\parallel} is much larger ($\Delta n_{\parallel} \sim 0.03$ for the same temperature rise). Under the same experimental situation, a diffraction efficiency of about 2×10^{-1} is observed (i.e., a ten-fold increase). At least a factor of two in the diffraction efficiency was also observed in thicker samples ($\approx 75 \mu\text{m}$).

The decay behavior of the diffractions (from the He-Ne) is depicted in Fig. 5(a) and (b), for the case where \vec{q} is normal to the director axis \vec{n} , and for \vec{q} parallel to \vec{n} , respectively. Since the grating constant is about $17 \mu\text{m}$ (for n_1) at a 2° cross angle, while the sample thickness is $40 \mu\text{m}$, the thermal diffusion may be approximated as a 1-dimensional problem along \vec{q} (for this crossing angle at least). In that case, the decay time constants are given by $\tau_1 = (D_1 q_1^2)^{-1}$ and $\tau_{11} = (D_{11} q_{11}^2)^{-1}$, respectively. Using the value $D_1 = 7.9 \times 10^{-4} \text{ cm}^2/\text{s}$, $D_{11} = 1.25 \times 10^{-3} \text{ cm}^2/\text{s}$, and $q_1^2 \sim (2\pi/17 \mu\text{m})^2$, and $q_{11}^2 \sim ((n_{11} \cdot 2\pi/n_1)/17 \mu\text{m})^2$; we get $\tau_1 \approx 110 \mu\text{s}$ and τ_{11} of $55 \mu\text{s}$. Experimentally, we obtain [from Fig. 5(a) and (b)] a value of $100 \mu\text{s}$ for τ_1 and $50 \mu\text{s}$ for τ_{11} , showing remarkable

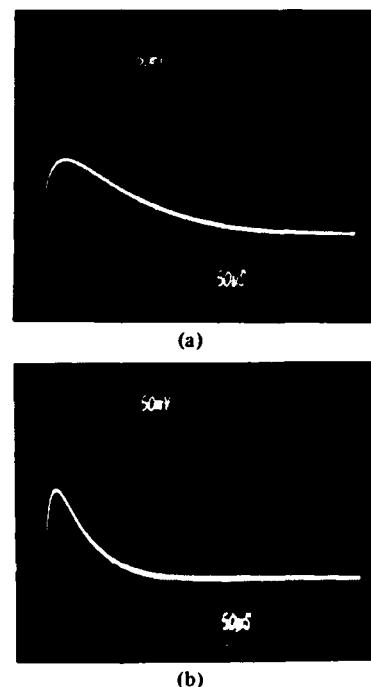


Fig. 5. (a) The decay of the thermal grating as monitored by the He-Ne diffraction. Time scale is $50 \mu\text{s}/\text{div}$. The grating wave vector \vec{q} is perpendicular to the director axis \vec{n} . (b) Thermal grating decay for \vec{q} parallel to the director axis \vec{n} . Decay is shorter by a factor of two.

agreement with the theoretical expectation. In general, the decay time constant decreases as we increase the wave-mixing angle θ (i.e., increase q), in a roughly q^{-2} dependence.

The rather large amount of pump energy needed to generate the observed diffraction is simply due to the fact that the liquid crystal used (PCB) absorbs very little at the pump laser wavelength ($0.53 \mu\text{m}$). The absorption can be easily increased by "doping" the PCB with traces of dissolved dyes. Using dyed samples, the same diffraction efficiency is observed using pump laser energies on the order of 3 or 4 mJ. A detailed study of both the rise and the decay of the diffraction shows that there is hardly any difference compared to the "undyed" or pure nematic. This indicates that the dye molecules essentially act as absorbers and rapidly transfer the excitation to the nematic via some intermolecular relaxation processes.

In the case of dyed samples, the sample shows sign of heating through the nematic \rightarrow isotropic transition at slightly elevated input energies ($>10 \text{ mJ}$). In that case, multiorder diffractions are observed. The decay is characterized by very long lifetime (cf., Fig. 6) on the order of $\sim 150 \text{ ms}$. This is consistent with the fact that when the input energies are high, grating or "line" of liquid are produced [22]. When these lines cool through the isotropic-nematic point, the orientations of the director axes will be random. These lines of nematics (with a refractive index (~ 1.58) higher than the surrounding nematic $n_1 \sim 1.52$) reorient themselves with a time constant characterized by the grating spacing λ_q of $17 \mu\text{m}$, (which is much smaller than the thickness of the sample $40 \mu\text{m}$). Using the well-known results for τ in terms of the viscosity ($\tau = \gamma \lambda_q^2 / K \pi^2$), we get a reorientation time of $\approx 290 \text{ ms}$ (using $K \sim 0.7 \times 10^{-8}$; $\gamma \sim 0.7$; $\lambda_q = 17 \mu\text{m}$) in support of the above experimental observation.



Fig. 6. The decay behavior of the thermal grating of a "dyed" PCB sample when the grating maxima give rise to liquid phase. Time scale is 50 ms/div. The observed relaxation time of ~ 150 ms is consistent with the theoretical prediction based on reorientation mechanisms.

FURTHER REMARKS

Time dependence studies of thermal effects in liquid crystals are both interesting (and new) and necessary.

Our study has resulted in the determination of several key parameters needed for a quantitative determination of the suitability and superiority over other materials, of nematics for pulsed laser wave-mixing processes. Since the thermal decay constants are on the order of microseconds, pulsed lasers of considerably less power can be employed (e.g., a 10 mJ, 10 μ s laser with a power of 1 kW) for wavefront conjugation or other purposes. Microsecond lasers also eliminate complications from acoustic waves interference. The versatility of nematics can be widened, and the pump energy requirement reduced, if appropriate dyes are dissolved in the nematics. Operating near T_c (but not too near to induce instability) will also obviously improve the diffraction efficiency. Experimentally we have verified that the diffraction increases by more than an order of magnitude at temperatures near T_c . Utilizing Δn_{11} will also improve the diffraction efficiency by at least an order of magnitude over Δn_1 , as we have demonstrated.

Using these new known experimental results on the dynamical constants of the wave-mixings and nematic parameters, we are currently investigating the actual optimum configurations for wavefront conjugation applications.

REFERENCES

- [1] I. C. Khoo, "Optically induced molecular reorientation and third order nonlinear processes in nematic liquid crystals," *Phys. Rev.*, vol. A23, pp. 2077-2081, 1981; see also I. C. Khoo and S. L. Zhuang, "Nonlinear light amplification in a nematic liquid crystal above the Freedericksz transition," *Appl. Phys. Lett.*, vol. 37, pp. 3-5, 1980; see also I. C. Khoo, "Theory of optically induced molecular reorientation and quantitative experiments on wave-mixings and self-focusing of light," *Phys. Rev.*, vol. A25, pp. 1636-1644, 1982.
- [2] S. D. Durbin, S. M. Arakelian, and Y. R. Shen, "Optically induced birefringence and Freedericksz transition in nematic liquid crystal," *Phys. Rev. Lett.*, vol. 47, pp. 1411-1415, 1981.
- [3] N. V. Tabiryan and B. Ya Zel'dovich, "The orientational optical nonlinearity of liquid crystals," *Mol. Cryst. Liq. Cryst.*, vol. 62, pp. 237-250; see also R. M. Herman and R. J. Serinko, "Nonlinear optical processes in nematic liquid crystals near a Freedericksz transition," *Phys. Rev.*, vol. A19, pp. 1757-1769, 1979.
- [4] I. C. Khoo and S. L. Zhuang, "Wavefront conjugation in nematic liquid crystals," *IEEE J. Quantum Electron.*, vol. QE-18, pp. 246-248, Feb. 1982; see also E. N. Leith, H. Chen, Y. Cheng, G. Swanson, and I. C. Khoo, "Wavefront conjugation with reduced coherence," in *Proc. 5th Rochester Conf. Coherence, Quantum Optics*, 1983.
- [5] I. C. Khoo, P. Y. Yan, T. H. Liu, S. Shepard, and J. Y. Hou, "Theory and experiment on optical transverse intensity bistability in the transmission through a nonlinear thin (nematic liquid crystal) film," *Phys. Rev.*, vol. A29, pp. 2756-2764, 1984; see also I. C. Khoo, J. Y. Hou, R. Normandin, and V. C. Y. So, "Theory and experiment on optical bistability in a Fabry-Perot interferometer with an intracavity nematic liquid crystal film," *Phys. Rev.*, vol. A27, pp. 3251-3257, 1983.
- [6] G. Barbero, F. Simoni, and P. Aiello, "Nonlinear optical reorientation in hybrid aligned nematics," *J. Appl. Phys.*, vol. 55, pp. 304-311, 1984; see also I. C. Khoo, "Optical-thermal induced total internal reflection to transmission switching at a glass-nematic liquid crystal interface," *Appl. Phys. Lett.*, vol. 40, pp. 645-648, 1982.
- [7] I. C. Khoo and S. Shepard, "Submillisecond grating diffractions in nematic liquid crystal films," *J. Appl. Phys.*, vol. 54, pp. 5491-5493, 1983.
- [8] F. J. Kahn, "IR-laser induced thermo-optic smectic liquid crystal storage displays," *Appl. Phys. Lett.*, vol. 22, pp. 111-113, 1973, and references therein; see also V. Volterra and I. Wiener Avnear, *Opt. Commun.*, "CW thermal lens effects in thin laser of nematic liquid crystal," *Opt. Commun.*, vol. 12, pp. 194-197, 1974.
- [9] G. Martin and R. W. Hellwarth, "Infrared-to-optical image conversion by Bragg reflection from thermally induced index gratings," *Appl. Phys. Lett.*, vol. 34, pp. 371-373, 1979.
- [10] I. O. Tocho, W. Sibbett, and D. J. Bradley, "Picosecond phase-conjugate reflection from organic dye saturable absorbers," *Opt. Commun.*, vol. 34, pp. 122-126, 1980; see also "Thermal effects in phase conjugation in saturable absorbers with picosecond pulses," *Opt. Commun.*, vol. 37, pp. 67-71, 1981; see also R. C. Caro and M. C. Gower, "Phase conjugation by degenerate four-wave mixing in absorbing media," *IEEE J. Quantum Electron.*, vol. QE-18, pp. 1376-1380, Sept. 1982; see also "Amplified phase conjugate reflection of krl laser radiation," *Appl. Phys. Lett.*, vol. 39, pp. 855-857, 1981.
- [11] M. H. Garrett and H. J. Hoffman, "Thermally induced phase conjugation efficiency and beam quality studies," *J. Opt. Soc. Amer.*, vol. 73, pp. 617-623, 1983.
- [12] I. C. Khoo and R. Normandin, "Nanosecond laser induced four-wave mixings and ultrasonic waves in nematic liquid crystal films," *Opt. Lett.*, vol. 9, pp. 285-287, 1984.
- [13] W. H. de Jeu, *Physical Properties of Liquid Crystalline Materials*. New York: Gordon and Breach, 1980, ch. 4 and references therein.
- [14] H. Hsiung, L. P. Shi, and Y. R. Shen, "Time dependent laser induced molecular reorientation in a nematic liquid crystal film," *Bull. Amer. Phys. Soc.*, vol. 29, p. 394, 1984; see also *Phys. Rev.*, vol. A30, pp. 1453-1459, 1984.
- [15] Using nanosecond laser pulses, we have observed degenerate four-wave mixing signals associated with the molecular reorientation nonlinearity in a homeotropic sample (for the case $\beta = 0$).
- [16] K. A. Nelson, R. J. Dwayne Miller, D. R. Lutz, and M. D. Fayer, "Optical generation of tunable ultrasonic waves," *J. Appl. Phys.*, vol. 53, pp. 1144-1149, 1982.
- [17] R. C. Desai, M. D. Levenson, and J. A. Barber, "Forced Rayleigh scattering: Thermal and acoustic effects in phase conjugate wavefront generation," *Phys. Rev.*, vol. A27, pp. 1968-1976, 1983; see also I. P. Battra, R. H. Enns, and D. Pohl, "Stimulated thermal scattering of light," *Phys. Status Solidi*, vol. 48, pp. 11-63, 1971.
- [18] R. G. Horn, "Refractive indices and order parameters of two liquid crystals," *J. de Phys.*, vol. 39, pp. 105-109, 1978; see for example, the refractive index of PCB at 6328 and 5890 A as a function of temperature.
- [19] G. R. Van Hecke and J. Stecki, "Pretransitional behaviour of the density of the nematic phase," *Phys. Rev.*, vol. A25, pp. 1123-1126, 1982; see also D. Armitage and F. P. Price, "Volumetric study of the nematic-isotropic pretransition region," *Phys. Rev.*, vol. A15, pp. 2496-2500, 1977.
- [20] N. A. Bloembergen, *Nonlinear Optics*. New York: Benjamin, 1965.
- [21] See, for example, M. E. Mack, "Stimulated thermal light scattering in the picosecond regime," *Phys. Rev. Lett.*, vol. 22, pp. 13-15, 1969, for some tabulated value of $\partial n/\partial T$; see also R. M. Herman and M. A. Gray, "The prediction of the stimulated thermal Ray-

leigh scattering in liquids," *Phys. Rev. Lett.*, vol. 19, pp. 824-828, 1967; see also R. W. Hellwarth, "Third order optical susceptibilities of liquids and solids," in *Progress in Quantum Electronics*, vol. 5, J. H. Sanders and S. Stenholm, Eds. New York: Pergamon, 1977, p. 1.

- [22] The effect is similar to the so-called "channels effect," observed by V. F. Kitaeva, N. N. Sobolev, A. S. Folot'ko, L. Csillag, and N. Kroo, "Light diffraction by laser beam created "channels" in nematic liquid crystals," *Mol. Cryst. Liq. Cryst.*, vol. 91, pp. 137-143, 1983; in the case of smectic sample, the reorientation upon supercooling is random, leading to permanent grating information; see also I. C. Khoo and R. Normandin, "Nanosecond laser induced ultrasonic waves and erasable permanent gratings in smectic liquid crystal," *J. Appl. Phys.*, vol. 55, pp. 1416-1418, 1984.



Iam-Choon Khoo (M'85) was born in Penang, Malaysia, in 1949. He received the B.S. degree in physics with a first class honors from the University of Malaya, Malaysia, in 1971, and the M.A. and Ph.D. degrees in physics from the University of Rochester, Rochester, NY, in 1973 and 1976, respectively.

He has held postdoctoral and research associate positions of Ames Laboratory, Iowa State University of Science and Technology, Ames, IA, the University of Southern California, Los Angeles, CA, and the University of Toronto, Ont., Canada. He then joined the Physics Department at Wayne State University, Detroit, MI,

in 1979 as an Assistant Professor, becoming an Associate Professor in 1983. In 1984, he joined the faculty at the Pennsylvania State University, University Park, PA, as an Associate Professor with the Department of Electrical Engineering. His current research interests are in theoretical and experimental nonlinear optical processes, optical wave mixing, wavefront conjugation, optical bistability, and switching in liquid crystalline materials.

Dr. Khoo is a member of the Optical Society of America.



Richard Normandin received the B.Sc. degree in physics from the Université de Montreal, Montreal, P.Q., Canada, in 1973. Subsequently, he obtained the M.Sc. degree for work in optical high-speed signal processing by surface acoustic wave interactions, and the Ph.D. degree in 1980 in the field of nonlinear optics in optical planar waveguides, both from the University of Toronto, Toronto, Ont., Canada.

He was previously with the solid-state physics section of the National Research Council of Canada, following a postdoctoral stay at Stanford University, Stanford, CA, with the support of the Natural Sciences and Engineering Research Council and the Rutherford Memorial Scholarship of the Royal Society of Canada. Currently, he is a research scientist with the National Research Council of Canada in the division of physics. His present interests are in the area of nonlinear optical properties of atoms near or at an interface, and their possible applications in quantum electronics.

Dr. Normandin is a member of the Canadian Association of Physicists, the Society of Photo-optical Instrumentation Engineers and the Optical Society of America.

Passive optical self-limiter using laser-induced axially asymmetric and symmetric transverse self-phase modulations in nematic liquid crystals

I. C. Khoo, G. M. Finn, R. R. Michael, and T. H. Liu

Department of Electrical Engineering, Pennsylvania State University, University Park, Pennsylvania 16802

Received October 11, 1985; accepted January 15, 1986

Using low-power cw lasers in conjunction with the symmetric and asymmetric nonlinear transverse self-phase modulation imparted by a nematic liquid-crystal film, we have demonstrated two forms of transverse intensity-switching and power-limiting operations. Applications to high-power nanosecond laser are also feasible.

The passage of a laser beam through a nonlinear medium is accompanied by interesting transverse optical intensity-redistribution phenomena, such as self-focusing, defocusing, ring formation, and beam breakup.¹ These processes have found applications in some optical devices,²⁻⁴ among them the so-called passive optical limiter.⁵

We report the experimental observation of two forms of optical intensity-switching processes associated with a transverse self-phase-modulation effect in a nematic liquid crystal first observed by Zolotko *et al.* and Durbin *et al.*⁶ In one case, the whole incident beam is involved, creating what we call a transversely symmetric self-phase modulation (SSPM). By imposing an asymmetry on the incident laser beam (e.g., by half blocking it), an asymmetric self-phase-modulation (ASPM) effect is induced.

Figure 1 is a schematic of the experimental setup used. The laser used is a cw linearly polarized Ar⁺ laser (0.5145- μm line). The liquid crystal used is a homeotropically aligned (cf. Fig. 2) (pentylcyanobiphenyl) (PCB) film. The configuration of the director axis \hat{n} , the optical electric field \mathbf{E}_{op} , and the propagation wave vector \mathbf{k} is such that large reorientational nonlinearity is induced.⁷ The laser-induced reorientation dielectric-constant change $\delta\epsilon(r)$ is given by⁷

$$\delta\epsilon(r) \sim \frac{\Delta\epsilon\pi^2 I_{\text{op}}(r)}{4 I_F} \sin^2 2\beta, \quad (1)$$

where I_F is the optical Freedericksz intensity⁷ [$I_F = (nc\pi^2 K/2\Delta\epsilon d^2)$]; $\Delta\epsilon$ is the optical dielectric anisotropy ($\Delta\epsilon = \epsilon_{11} - \epsilon_{\perp}$, where ϵ_{11} and ϵ_{\perp} are the optical dielectric constant for field polarization parallel to and perpendicular to the director axis, respectively); K is the elastic constant; and d is the thickness of the sample.

In terms of the refractive-index change δn , we have

$$\delta n(r) = n_2 I(r) = (\Delta\epsilon\pi^2/4nI_F) \sin^2 2\beta I_{\text{op}}(r). \quad (2)$$

If the incident laser beam is half blocked (e.g., beginning in the positive x direction), then, roughly, these two expressions will be multiplied by a step function $\theta(x)$ [$\theta(x) = 0, x < 0; \theta(x) = 1, x > 0$]. The

liquid-crystal film has a thickness of 75 μm . In this case, the effect of the transverse nonlinearity is to impart an intensity-dependent phase shift on the laser beam. This phase shift leads to external self-focusing (and the associated change in the laser-beam divergence) in the case of SSPM or to self-deflection in the case of ASPM.

For a given radially symmetric incident optical electric-field distribution at the plane of the nonlinear film, $I_0(r, 0)$, the transmitted field at a distance z , $E(r, z)$, is simply given by the usual diffraction integral,³

$$I(r, z) = \left(\frac{2\pi}{\lambda z}\right)^2 \left| \int_0^\infty \sqrt{I_0(r)} dr r J_0(2\pi r r_0/\lambda z) \times \exp\left\{-ik\left[\frac{r^2}{2z} + \frac{r^2}{2R} + \delta n(r)d\right]\right\} \right|^2;$$

where $\sqrt{I_0(r)}$ is the incident electric-field amplitude, R is the radius of curvature, d is the thickness of the nonlinear thin film, and λ is the wavelength of the laser.

Obviously, the intensity distribution $I(r, z)$ depends on several parameters. Most importantly, if the input laser beam is Gaussian [i.e., if $I_0(r, 0) \sim I_0 \exp -2r^2/w_0^2$, where w_0 is the beam waist], then the far-field intensity distribution in the case of SSPM will yield

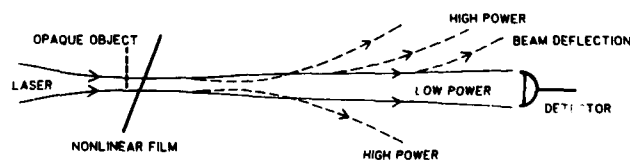


Fig. 1. Schematic of the experimental setup for symmetric and asymmetric (with the use of the opaque object to half block the laser) self-phase-modulation effect. Symmetric self-phase modulation gives rise to self-focusing and divergence of the laser at the detector plane at high power, as shown by the dashed lines. Also shown by dashed lines is the self-bending effect associated with asymmetric self-phase modulation.

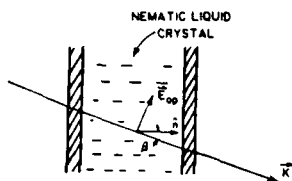
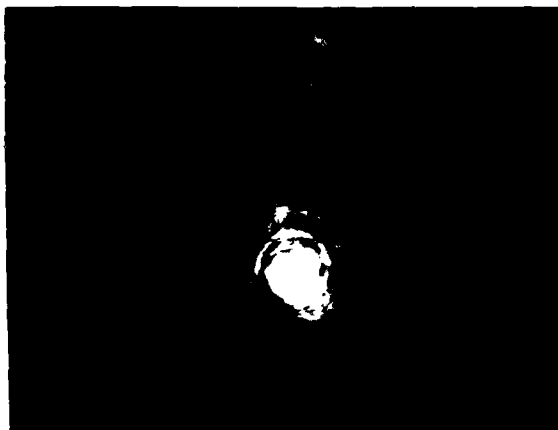


Fig. 2. Optical propagation in a homeotropic nematic crystal film.



(a)



(b)



(c)

Fig. 3. (a) Photograph of the laser at the detector plane at low power. (b) Photograph of the laser at higher power showing ring formation and increased divergence for the case when the incident laser has a positive radius of curvature. The central portion remains bright for the full laser-power range. (c) Photograph of the laser at the detector plane at high power for the case when the incident laser has a negative radius of curvature. The central portion tends to be dark for the entire power range.

interference rings at high input intensity. Moreover, the divergence of the beam will also change drastically. This is observed in our experiment and in other studies.^{3,6} In the case of ASPM, the asymmetry in the self-phase modulation (in the x direction for the present case) gives rise to self-bending of the beam besides the other effects associated with SSPM mentioned above.

The photograph in Fig. 3(a) is that of the laser beam (detected at a plane located 7 m from the sample) at low power, where there is no appreciable self-phase-modulation effect. At high intensity (~ 100 W/cm²), both diffraction rings and a drastic increase in the divergence of the laser are observed [cf. Figs. 3(b) and 3(c)].

As the sample is moved around the focal plane of the lens L_1 (i.e., the radius of curvature R of the wave front changes in sign as well as in magnitude), the intensity distribution at the detector plane varies considerably.⁸ Figure 3(b) is typical of the intensity distribution if the sample is located just beyond the focal plane of L_1 , i.e., if R is positive.

The central portion, i.e., the on-axis part of the beam, has a small region of brightness that seems to persist at all input intensities. On the other hand, Fig. 3(c) is typical of the intensity distribution if the sample is located before the focal plane of L_1 . The central region is dark at high-input laser intensity. These are obviously diffraction effects, coupled with the nonlinear transverse phase shift.

As a result of the drastic increase in the divergence of the beam at the detector plane, the detected power (the so-called output) versus the input laser power will deviate from linear, tending to a so-called "limiting" form. This is indeed observed, as is shown in Fig. 4. The detector collects almost all the transmitted laser beam, at low power. But at higher intensity, the output shows limiting behavior even as the input is increased by almost 10 times.

In the case of ASPM, similar ring formation and laser-divergence change are observed, with an additional effect that the whole beam bends toward the negative X direction.⁹ Figures 5(a) and 5(b) show such a deflection effect. The beam moves by a displacement of roughly twice the laser-beam waist at the observation plane. The experimentally observed deflection angle is found to be 0.03 rad. Using Eq. (2), one can estimate this deflection angle. For the liquid

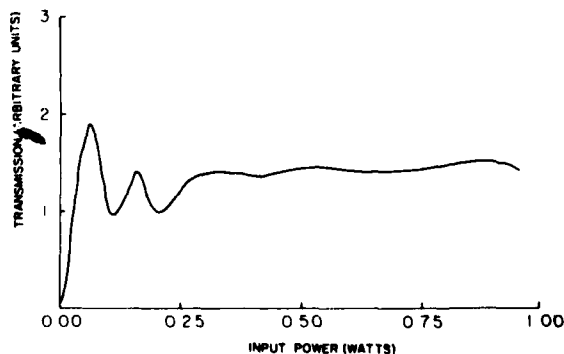
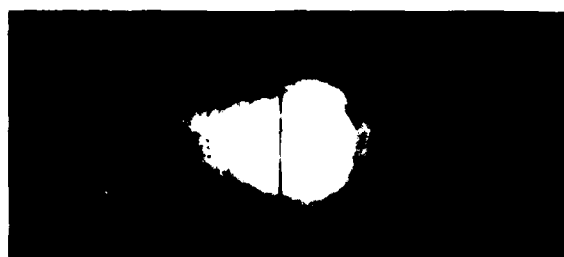


Fig. 4. Plot of the detector power versus the incident laser power showing power-limiting effect.



(a)



(b)

Fig. 5. (a) Photograph of the laser spot on the observation plane at low power. Black line at center is for reference purpose. (b) Same as in (a), but at high power. The beam deflects by a displacement of about twice the laser-beam waist.



Fig. 6. Photograph of the increased divergence and ring formation due to nanosecond laser-induced self-phase modulation.

crystal used in the deflection experiment, the thickness $d = 100 \mu\text{m}$ and $\beta = 15^\circ$, I_F is about 500 W/cm^2 (using $\Delta\epsilon = 0.8$, $\epsilon \sim 2.25$, $K = 0.8 \times 10^{-6} \text{ dyn}$). The optical intensity used is 100 W/cm^2 . From Eq. (2), then, we get $\delta n(r=0) \simeq 0.06$. The half-block laser has a radius of about 0.05 cm . The refractive-index coefficient is therefore about $0.06 - 0.05 \sim 1.2 \text{ cm}^{-1}$. The deflection angle θ associated with this index coefficient is therefore given by $\theta \sim 0.07 \text{ rad}$. This is close to the experimentally observed value in view of several factors of unity overestimation in the theory.

Molecular reorientation in nematics can also be induced by high-power nanosecond lasers. Hsiung *et al.*¹⁰ had shown that a homeotropic nematic liquid crystal will be reoriented by a normally incident nanosecond laser pulse, provided that a strong dc bias magnetic field is present, in analogy to the cw case.⁷ In our experiment, the nanosecond laser pulse (*Q*-switched Nd:YAG second harmonic; 20-nsec duration; 10 mJ; 1-mm^2 beam size) is incident at a nonnormal angle as in Fig. 2. In this case, molecular reorientation will occur *without a bias field*, in analogy again to the cw case.⁷ Furthermore, we use a nematic liquid crystal (EM chemicals EK46) at a temperature far below the nematic \rightarrow isotropic point to minimize the thermal contribution. External self-focusing effect and also the formation of ring structures associated with SSPM are observed. Figure 6 is a photograph of the transmitted (single-shot) laser pulse. A coincident cw He-Ne laser also shows similar far-field diffraction effects that collapse back to the original laser-beam profile in about 4 or 5 sec, which is the orientational relaxation time characteristic of the $75\text{-}\mu\text{m}$ sample used.⁷ An output-versus-input plot also shows power-limiting behavior similar to that shown in Fig. 3.

This research is supported in part by grant ECS 8415387 from the National Science Foundation and grant 840375 from the U.S. Air Force Office of Scientific Research. Some helpful discussions with A. E. Kaplan on laser self-bending effect are also acknowledged.

References

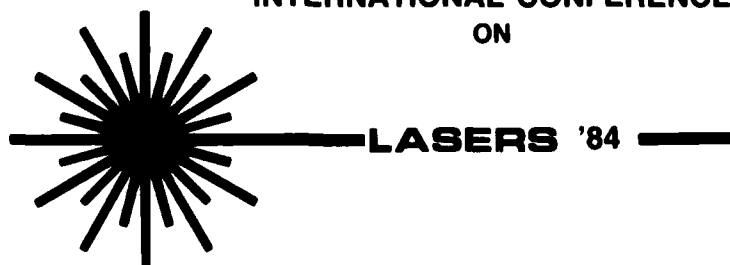
1. See, for example, J. F. Reintjes, *Nonlinear Optical Parametric Processes in Liquids and Gases* (Academic, New York, 1984), Chap. 5 and references therein.
2. J. E. Bjorkholm, P. W. Smith, W. J. Tomlinson, and A. E. Kaplan, *Opt. Lett.* **6**, 345 (1981).
3. I. C. Khoo, *Appl. Phys. Lett.* **41**, 909 (1982); I. C. Khoo, T. H. Liu, P. Y. Yan, S. Shepard, and J. Y. Hou, *Phys. Rev. A* **29**, 2756 (1984).
4. K. Tai, H. M. Gibbs, N. Peyghambarian, and A. Mysyrowicz, *Opt. Lett.* **10**, 220 (1985).
5. M. F. Soileau, W. E. Williams, and E. W. Van Stryland, *IEEE J. Quantum Electron.* **19**, 731 (1983); T. F. Boggess, Jr., A. L. Smith, S. C. Moss, I. W. Boyd, and E. W. Van Stryland, *IEEE J. Quantum Electron.* **QE-21**, 488 (1985); J. A. Hermann, *J. Opt. Soc. Am. A* **1**, 729 (1984), and references therein.
6. A. S. Zolotko, V. F. Kitaeva, N. Kroo, N. N. Sobolev, and L. Chillag, *JETP Lett.* **32**, 158 (1980); S. D. Durbin, S. M. Arakelian, and Y. R. Shen, *Opt. Lett.* **6**, 411 (1981).
7. I. C. Khoo, *Phys. Rev. A* **23**, 1636 (1981); **25**, 1636 (1982); **26**, 1131 (1983); **27**, 2747 (1983); see also I. C. Khoo and Y. R. Shen, *Opt. Eng.* **24**, 579 (1985), and references therein.
8. E. Santamato and Y. R. Shen, *Opt. Lett.* **9**, 564 (1984).
9. A. E. Kaplan, *JETP Lett.* **9**, 33 (1969); *Opt. Lett.* **6**, 360 (1981).
10. H. Hsiung, L. P. Shi, and Y. R. Shen, *Phys. Rev. A* **30**, 1453 (1984).

TRANSVERSE SELF-PHASE MODULATION OPTICAL
BISTABILITY

I. C. Khoo

pp. 196-201

REPRINTED FROM
PROCEEDINGS
OF THE
INTERNATIONAL CONFERENCE
ON



LASERS '84

TRANSVERSE SELF-PHASE MODULATION OPTICAL BISTABILITY

I. C. Khoo
Electrical Engineering Department
University Park, PA 16802

Abstract

We present here further analytical results for the fundamental mechanisms of bistable transverse intensity distribution of a Gaussian laser beam after its passage through a thin nonlinear medium. We have derived explicit analytical expressions for the transmitted intensity distribution in the case where the beam undergoes only self-phase modulation effects and where a single reflection feedback is present. The geometrical conditions for bistable optical switching, the dependences on various geometrical and laser parameters for both positive and negative nonlinearities, and the effect of saturation, are discussed.

Introduction

Recently, a new class of so-called cavity-less optical bistability phenomenon has received considerable attention. In particular, Kaplan¹ has proposed several schemes for optical bistability utilizing the self-focusing process, in conjunction with a single reflection feedback. A detailed theory² with experimental observations for the case of "weak" or "external" self focusing involving a nonlinear thin film has recently been described.

In this paper, we present further new analytical results for this type of optical bistability, which originates from the transversely dependent nonlinear phase shift experienced by a Gaussian laser beam in traversing the nonlinear thin film. We generalize the theoretical consideration to both positive and negative nonlinearities (i.e. for $n_2 > 0$ and for $n_2 < 0$) and derive explicit expressions for the conditions for bistable operation. The theory presented here should be applicable to all nonlinear thin film, and in particular, solid-state thin films which appear to be the best candidate for optical processing applications.

Theory

The configuration for the observation of transverse intensity bistability is schematically depicted in Figure 1. A cw laser with a curvature R , incident on the nonlinear thin film (where the laser beam waist is ω) is reflected after passage through the film and a lens back onto itself. The transmission through the mirror is monitored by a pin-hole placed at various radial positions from the axis of the beam. The refractive index change induced on the film is of the form

$$\Delta n = n_2 I(r) \quad (1)$$

where $I(r)$ is the optical intensity at the film and n_2 is the nonlinearity coefficient. Typically, $n_2 \sim 10^{-9}$ for a liquid crystal film, and of the same magnitude or larger for solid-state thin film.

This refractive index change imparts a transverse phase shift on the optical field.

$$\delta\phi(r) = \frac{2\pi}{\lambda} \int_0^d n_2(z) I(r) dz = \frac{2\pi}{\lambda} n_2 d I(r) \quad (2)$$

where d is the thickness of the nonlinear film. The total optical intensity on the sample is given by the sum of the forward propagating and backward propagating (reflected) beam

$$I = I_o + I_R \quad (3)$$

Without loss of generality, and for the sake of clarity, we will ignore the presence of the lens. (The effect of including the lens is to introduce a geometrical factor and will be discussed in a later section). In this case, the exit beam electric field at a distance z from the nematic field is given by

$$E(r_o, z) = \frac{2\pi}{i\lambda z} \exp(ikz) \exp\left\{-\frac{ikr_o^2}{2z}\right\} \int_0^\infty E_o(r, 0) \exp\left\{-\frac{ikr^2}{2z}\right\} J_0\left[\frac{2\pi r r_o}{\lambda z}\right] \exp[-i\delta\phi(r)] r dr \quad (4)$$

where $r_0 = (x_0 + y_0)^{1/2}$ and $r = (x^2 + y^2)^{1/2}$ and J_0 is the zeroth-order Bessel Function. The incident laser beam is assumed to be a Gaussian, and its electric field is given by

$$E_0(r, 0) = \sqrt{I_0} \exp \left[-\frac{r^2}{2} - \frac{ikr^2}{2R} \right] \quad (5)$$

The output intensity at z is given by squaring both sides of equation (4) to give

$$I(r_0, z) = \left[\frac{2\pi}{\lambda z} \right]^2 I_0 \left| \int_0^\infty dr r J_0(2\pi r r_0 / \lambda z) \exp(-r^2/\omega_0^2) \times \exp \left[-ik \left(\frac{r^2}{2z} + \frac{r^2}{2R} + \bar{n}_2 I_0 d \exp \left[-\frac{2r^2}{\omega^2} \right] + \bar{n}_2 R_m d I(r, z) \right) \right] \right|^2 \quad (6)$$

Notice from (6) that it is an integral equation for the intensity distribution $I(r, z)$. The possibility of bistable or multistable intensity distribution is therefore obvious. It is not possible to get a closed-form solution for $I(r, z)$ from (6). We found that, however, by making very reasonable approximations, we can convert equation (6) to a set of very simple transcendental algebraic equations from which much insight about the bistable operation can be gained. The approximation employed can be shown to be equivalent to the lens approximation, and consist of the simple procedure of expanding $I(r_0, z)$ as well as I_0 and I_1 in the form

$$I(r_0, z) = \sum_{n=0}^{\infty} (-1)^n A_{2n} r_0^{2n} \quad (7)$$

and retaining only the first two terms. [We have shown in previous work that it is possible to redo the problem by including all the terms for the forward propagating field (corresponding to I_0), but the result for the bistable switching is not appreciably changed]. Following reference 2, we let,

$$A_0 = \frac{I_0}{4z^2 \left[\left(\frac{1}{\omega^2 k} \right)^2 + \left(\frac{1}{2z} + \frac{1}{2R} - \frac{2n_2 I_0 d}{\omega^2} - n_2 d R_m A_2 \right)^2 \right]} \quad (8)$$

and, by introducing a unitless parameter u

$$u = \omega^2 k (1/2z + 1/2R - 2n_2 I_0 d / \omega^2 - n_2 d R_m A_2) \quad (8a)$$

the solutions for A_0 and A_2 are given by the solution for u in the equation

$$B_1 - B_2 u = \frac{1}{(1+u^2)^2} \quad (9)$$

where

$$B_1 = \frac{3z^4 (1/2z + 1/2R - 2n_2 I_0 d / \omega^2)}{R_m n_2 I_0 d \cdot 6k^4} \quad (10)$$

and

$$B_2 = \frac{8z^4}{R_m n_2 I_0 d \cdot 8k^5} \quad (11)$$

Figure (2) is a plot of the function $B_1 - B_2 u$ (L.H.S. of (9)), and $(1 + u^2)^{-2}$ (R.H.S. of (9)). Where there are triple intersection points correspond to the bistable switching region.

Discussion

Before we proceed to discuss the geometrical significance and conditions deducible from Figure (2), it is instructive to note here that aside from the expected dependence of B_1 and B_2 on z , and the radius of curvature R , both B_1 and B_2 are extremely sensitive to the beam waist of the incoming laser beam. $B_1 \propto \omega^{-6}$ while $B_2 \propto \omega^{-8}$. On the other hand, the existence of the triple-value solutions from Figure 2 is clearly dependant on the value of B_1 and B_2 . This implies of course that transverse optical bistability is extremely sensitive to the incoming laser beam waist. Such a dependence is actually experimentally verified in our study of transverse optical bistability involving a nematic

liquid crystal film, and is expected to hold true too for other thin film with nonlinearity of the form given in (1).

There is a similarity between Figure (2) and the usual Fabry-Perot optical bistability treatment. Both involve solving for triple valued quantity from the intersection of a straight line and a bell-shaped function. The slope of the straight line is inversely proportional to the optical intensity of the incoming beam. The difference in the present case is that only one (as opposed to the usual Fabry-Perot, which involves infinite, periodic) bell-shaped function is involved. Also, the intercept of the straight line with the "u" axis also changes with the beam intensity.

Figure (2) allows one to deduce the geometrical conditions for observing bistability. When $I_0 = 0$, slope $-B_2$ (denoted as m) is infinite, while the intercept (denoted as $B_x = B_1/B_2$) is given by

$$B_x = \frac{2k}{\omega^2} \left(\frac{1}{2z} + \frac{1}{2R} - 2n_2 I_0 d/\omega^2 \right) \quad (12)$$

Consider the case $n_2 > 0$. If I_0 is increased, then B_x will move towards $u = 0$, i.e. decreases, as shown in Figure 2. At the same time, the slope m will decrease in magnitude (m is still negative). In order for triple-valued solution to occur, a sufficient condition is that the magnitude of the slope must be less than the maximum magnitude of the tangent to the bell-shaped function on the positive u side. Let the corresponding optical intensity be denoted I_c i.e.

$$m(I_c) > -1.04 \quad (13)$$

where 1.04 is the maximum magnitude of the tangent to the bell-shaped function.

Correspondingly, the intercept is given by

$$b_{xc}(I_c) = 1.12 \quad (14)$$

A necessary condition for bistability is that $b_x(I=0) \geq 1.12$. From (14), we get

$$I_c = \frac{1}{2n_2 d k} \left[\frac{2k}{\omega^2} \left(\frac{1}{z} + \frac{1}{R} \right) - 1.12 \right] \quad (15)$$

And from (13), we get the sufficient condition for bistability as

$$\frac{8z^4}{R_m n_2 d \frac{8k^5}{2n_2 d k} \left[\frac{2k}{\omega^2} \left(\frac{1}{z} + \frac{1}{R} \right) - 1.12 \right]} \quad (16)$$

The square-bracket term in the denominator of (16) is positive by virtue of the fact that $b_x(I=0) \geq 1.12$. From (16), we have

$$\frac{1}{R} > \frac{30.8}{R_m} \frac{z^4}{(\omega^2 k)^5} + \frac{2.24}{\omega^2 k} - \frac{1}{z} \quad (17)$$

where R_m is the reflectivity of the feedback mirror.

Notice that n_2 cancels out exactly in the denominator of (16). The condition for optical bistability is independent of the magnitude of n_2 ! From (17), we see that transverse optical bistability is clearly a geometrical effect, depending only on the geometrical parameter like z and R . Equally noteworthy is the extreme sensitivity of the condition on the ω .

For the case of negative nonlinearity ($n_2 < 0$), the same argument can be pursued in an almost mirror-image fashion of Figure 3, leading to the conditions

$$b_x^-(I_c) = -1.12 \quad (18)$$

$$m^-(I_c) < 1.04 \quad (19)$$

This gives

$$I_c = - \frac{1}{2 |n_2| dk} \left[\frac{\omega^2 k}{2} \left(\frac{1}{z} + \frac{1}{R} \right) + 1.12 \right]$$

and, finally, the sufficient condition for bistability is

$$\frac{1}{R} < - \left[\frac{30.8z^4}{Rm(\omega^2 k)^5} + \frac{2.24}{\omega^2 k} + \frac{1}{z} \right] \quad (20)$$

Again, the condition is independent of the magnitude of n_2 , although it does reflect the sign of the n_2 by imposing the requirement that the radius of curvature of the incoming laser beam be negative.

In the presence of a lens between the thin film and the mirror, the analysis is straightforward though lengthy. Following Reference 2, the solutions for the output intensity (A_0 and A_2) can again be obtained by solving an equation of the form²

$$B_1 - B_2 V = (1 + V^2)^{-2} \quad (21)$$

where

$$B_1 = \frac{D_1^4}{2b_1^2 b^4 I_0 \omega^6 n_2 d R_m} \left[\frac{1}{2z} + \frac{1}{2R} - \frac{2n_2 I_0 d}{\omega^2} + \frac{ab}{kD_1} \right] \quad (22)$$

and

$$B_2 = \frac{D_1^4}{2b_1^2 b^4 I_0 \omega^8 n_2 d R_m k} \quad (23)$$

and $a = k/2z - k/2R$, $b = (k/2z)^2$ and $D_1 = b_1 - a_1 a$ ($b_1 = (k/2z_1)^2$ and $a_1 = k/2z_2 - k/2f$). Obviously ab/kD_1 , appearing in B_1 is a purely geometrical quantity. The similarity between the set of equation (21)-(23), and the set (9)-(11), not surprisingly, again leads to conditions for bistability that are independent of the magnitude of n_2 , and are dependent only on the various geometrical factors. For $n_2 > 0$, we have, for example

$$\frac{D_1^4}{-b_1^2 b^4 \omega^8 \left[\frac{\omega^2 k}{2} \left(\frac{1}{z} + \frac{1}{R} + \frac{ab}{kD_1} \right) - 1.12 \right]} < 1.04 \quad (24)$$

Although we have not conducted a thorough experimental investigation of how these conditions are obeyed, the geometric parameters used in our experimental observation of transverse bistability are within the prescribed conditions. We have deliberately experimented with set-ups that fall outside the condition for bistability and have not observed any switching. The preceding discussion also brings forth a hitherto neglected consideration, namely, the nonlinear response of the thin film does not necessarily have the same shape and/or width as the transverse dependence of the incident laser. Under cw illumination, diffusion processes (in solid state material) or nonlocal long-range interaction (e.g. in liquid crystal) will in general broaden the response. It becomes critical in view of the extreme dependence of the transverse bistability on the laser beam width, and the width of the response, therefore, to calculate exactly the transverse response of the material when these diffusive types of processes are present. Work is currently underway in this direction.

The theory as outlined above, and detailed in Reference 2, can be applied in the study of the effect of saturation, which has hitherto not been addressed to in the case of external or "weak" self focusing bistability. Saturation of the optical nonlinearity can assume many forms, depending on the corresponding physical processes involved. It is concomitant with the extraordinary large optical nonlinearity observed in materials like nematic liquid crystal films (molecular reorientational nonlinearity), solid state multi-quantum well structures (excitonic absorption) and sodium vapors (electronic resonances).

We have investigated several forms of saturation behaviour and how they affect the transverse bistability switching process. One of the most commonly occurring form is such

that the optically induced refractive index change is given as in Equation (1), but with n_2 replaced by an intensity dependent coefficient $n_2(I)$.

$$n_2(I) = \frac{n_2}{1 + I(r)/I_s} \quad (25)$$

where I_s is the saturation intensity. Details of our calculation are clearly outside the scope of the present paper. It suffices to note here that one could proceed with the same expansion procedure as outlined here and Reference 2 to obtain again two algebraic equations for A_0 and A_2 (c.f. Equation (8)). However, it is no longer possible to derive simple explicit analytical expressions for the conditions for bistability operations. Nevertheless, these algebraic equations can be very easily solved numerically. An interesting theoretical result, which occurs at a small range of saturation intensity, is depicted in Figure 3. The calculation uses the geometrical parameters similar to the set used in the experimental observation described in Reference 2, with an assumed saturation intensity I_s value near the switch-up point. As clearly depicted in Figure 3, two very closely bistability loops appear. The first loop occurs at a lower intensity, and is almost identical to one obtained with ($I_s = \infty$). The second loop occurs right after the switch-up point in the first loop, and the direction of switching is opposite to the initial loop. As we emphasized earlier, the occurrence of these two closely loop holds true only for a small range of I_s . At other values of I_s , the two bistability loops either merge into one, or break up into one bistability loop and a unidirectional "dip" at the higher intensity point.

Acknowledgement

I am indebted to T. H. Liu and R. Normandin for some assistance in the numerical computation. This research is supported by a grant from the National Science Foundation under grant number ECS8415387 and the Air Force Office of Scientific Research AFOSR 840375.

References

1. A. E. Kaplan, Opt. Letts. 6, 360 (1981)
2. I. C. Khoo, P. Y. Yan, T. H. Liu, S. Shepard and J. Y. Hou, Phys. Rev. A29, 2756 1984; see also references therein for a more complete list of references on similar work.

Figure Captions

- Figure 1. Schematic of the experimental set up for observing transverse intensity bistability. m: mirror; p: pinhole; NF: nonlinear thin film; $Z = 2(Z_1 + Z_2)$.
- Figure 2. Plot of the functions $B_1 - B_2 u$ and $(1+u^2)^{-2}$. B_x and B_{xc} are intercepts of $B_1 - B_2 u$ with the u -axis. m is the tangent to the bell-shaped function $(1+u^2)^{-2}$.
- Figure 3. Theoretical bistability output versus input plot for the on-axis region.

Fig.1

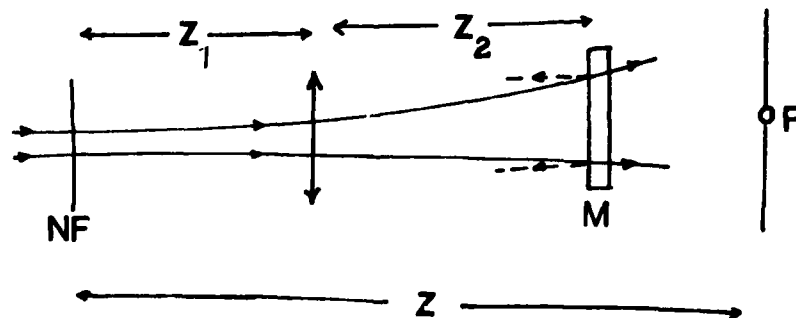


Fig.2

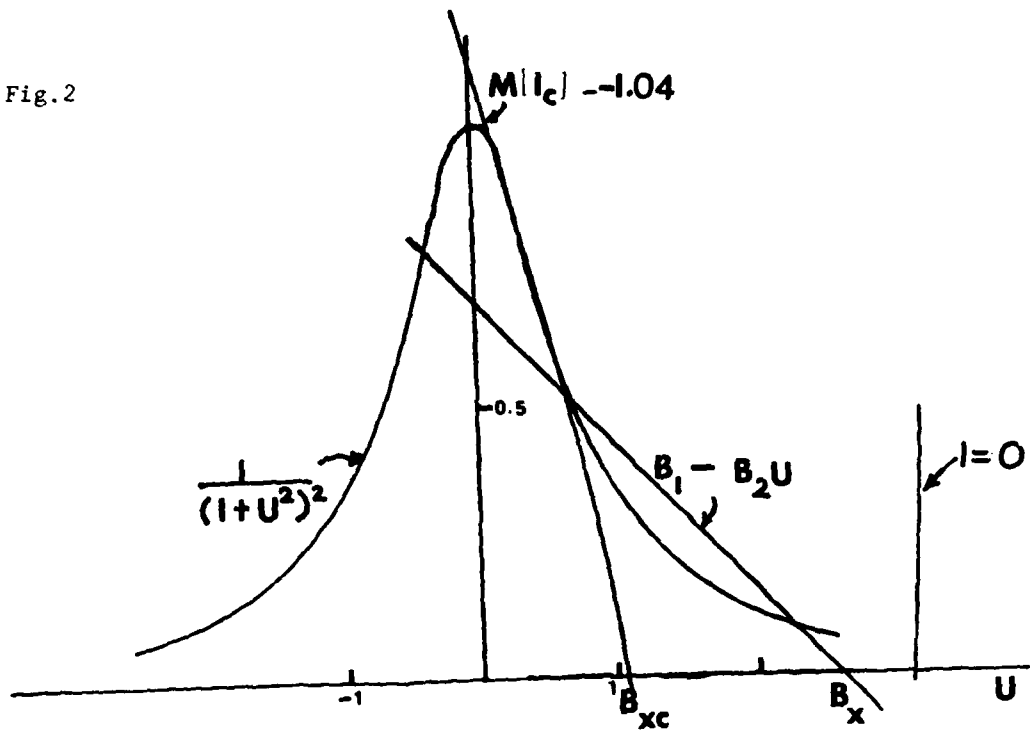
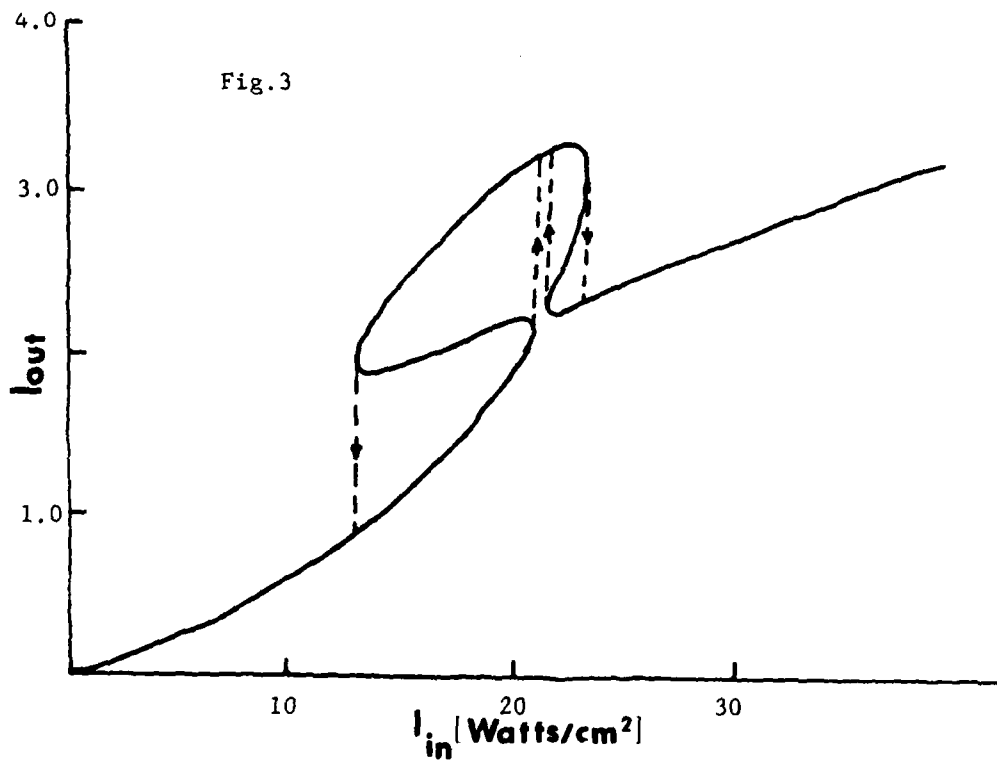


Fig.3



Wave front conjugation with gain and self-oscillation with a nematic liquid-crystal film

I. C. Khoo

Department of Electrical Engineering, The Pennsylvania State University, University Park, Pennsylvania 16802

(Received 15 July 1985; accepted for publication 12 August 1985)

We have observed for the first time wave front conjugation with amplified reflection return using the thermal nonlinearity of a thin film of nematic liquid crystal in conjunction with a low power laser (intensity on the order of 25 W/cm²). Self-oscillation is also observed.

Wave front conjugation, and the associated phenomena of imaging through aberration, amplified reflections, and other useful adaptive optical processes have been vigorously studied in the last few years.¹ Materials for wave front conjugation include sodium vapor, semiconductor crystals, barium titanate, electro-optic crystals (BSO), various liquids, liquid crystals, and others. The basic mechanism for nonlinearity ranges widely. In some materials the nonlinearity is sufficiently large for amplified reflection of the probe beam, leading to self-oscillations.² Such an effect has important applications in image amplification, laser designs, and other adaptive optics processes.

In nematic liquid crystal, there are two basic mechanisms for optical nonlinearities³⁻⁵ that have been used for degenerate four-wave mixing processes: optically induced refractive index change associated with the director axis reorientation, and laser induced thermal index effect. The fundamental mechanisms for these processes have been quantitatively documented. Application of these nonlinearities for wave front conjugation,⁶ where the aberration correction and speckle noise reduction (with spatially partially incoherent lasers) have also been demonstrated. In this letter we report the first successful demonstration of wave front conjugation with gain and self-oscillation, using the thermal nonlinearity in a nematic film in conjunction with low power cw (chopped) lasers.

Consider two linearly polarized lasers propagating through a homeotropically aligned nematic liquid crystal as shown in Fig. 1(a). The two beams are crossed at a small wave mixing angle θ in a plane perpendicular to the paper. For this geometry the refractive index as seen by the optical wave is given by

$$n_e = \frac{n_i n_o}{(n_o^2 \cos^2 \beta + n_i^2 \sin^2 \beta)^{1/2}} \quad (1)$$

for $\beta = 0$, $n_e = n_i$. On the other hand, if $\beta = 90^\circ$, e.g., using a planar-aligned nematic as shown in Fig. 1(b), $n_e = n_o$. Both n_i and n_o are strongly dependent on the temperature. At temperature removed from the nematic-isotropic transition temperature T_c , the magnitudes of dn_i/dT (positive) and dn_o/dT (negative) are already as large as most high index liquids ($\approx 2 \times 10^{-4} \text{ K}^{-1}$). As the temperature approaches T_c , both increase by more than an order of magnitude. As a consequence of this large nonlinearity, visible diffractions (with efficiency on the order of one percent or more) can be obtained by mixing two milliwatt cw lasers,⁷ using the natural absorption of some nematic [e.g., methoxy

benzylidene *p*-*n*-butylaniline (MBBA)] at the laser wavelength (5145 Å).

Another important characteristic of thermal grating formation in nematic is the relatively faster response. If the two incident lasers are chopped, there are two distinct components in the diffraction. (See Khoo and Shepard in Ref. 5.) One component rises instantaneously with the laser corresponding to a local heating at the interference intensity maxima at the sample. The other component, which is much slower, corresponds to an overall heating of the sample due to thermal diffusion from the grating maxima to the minima; the overall heating raises the temperature of the sample, and therefore increases the change in the refractive index. This overall heating of the sample is quite detrimental to the grating diffraction process if it raises the temperature of the sample over T_c , when the grating diffractions practically vanish. In our study, the duty cycles and duration of chopped cw lasers are adjusted such that the diffraction is maximized while minimizing the overall heating, as discussed in Ref. 5.

The process of laser induced thermal index change and the diffusion process (either in the liquid-crystal medium or through the cell walls) is a complicated three-dimensional problem. In ordinary liquids or in crystals, the fundamental parameters are the temperature T and the density ρ . In liquid

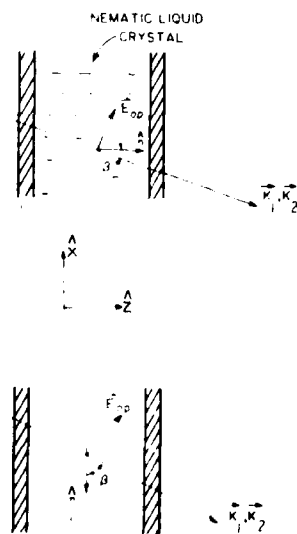


FIG. 1. Schematics of laser interaction in (a) a homeotropically aligned and (b) a planar aligned nematic liquid-crystal film. K_1 (probe beam) K_2 (pump beam) are the propagation wave vectors. E_1 and E_2 are the optical field vectors. The two laser beams intersect in a plane perpendicular to the paper.

crystal, one has also to include the order parameter S . If the chopped laser pulse durations are on the order of milliseconds, one would expect the density fluctuations in the sample to equilibrate, and we are thus left with S and T . The interplay between S and T , and the refractive indices n_1 and n_2 have been dealt with in a recent article. (See Khoo and Normandin in Ref. 5.) For our purpose here one may simplify the consideration by adopting T as the working parameter, described by the usual thermal diffusion equation

$$\rho c_v \frac{\partial T}{\partial t} - k \nabla^2 T = \frac{n c \alpha}{4\pi} E_{op}^2, \quad (2)$$

where ρ is the density of the nematic, c_v the specific heat, k the diffusion constant, n the refractive index, α the absorption constant, and E_{op} is the amplitude of the optical electric field. Both ρ and c_v are strongly temperature dependent, especially near T_c . However, their influence on the refractive index may be viewed as secondary; the primary effect comes from the change in T .

The total optical electric field E_{op} incident on the sample is made up, of course, of the contribution from the probe (E_1) and the pump beam (E_2). Their interference gives rise to an oscillating term $E_1 E_2 \cos qy$, where q is the grating wave vector ($q = 2\pi/\lambda_q$; $\lambda_q = \lambda_{op}/2 \sin(\theta/2)$, θ : wave mixing angle in the nematic), and y is the coordinate perpendicular to $\mathbf{K}_1 - \mathbf{K}_2$. If the incident lasers are pulsed, with pulse lengths shorter than all the thermal diffusion time constants (characteristics of diffusion time between the intensity maxima and the minima, and between the center plane of the liquid-crystal cell and the cell walls etc.), then the change in temperature ΔT [from Eq. (1)] is simply given by

$$\Delta T = \frac{\alpha}{\rho c_v} U(y), \quad (3)$$

where U is the energy of the laser pulse. On the other hand, if the laser pulses are longer than the diffusion time (which is true for our experiment using chopped cw lasers; laser pulses ≈ 100 ms, diffusion time constant ≈ 5 ms), then the spatial redistribution of the absorbed energy and the rise in temperature is obviously a complicated three-dimensional problem, a complete solution of which is clearly outside the scope of this letter. Nevertheless, in the steady state ($\partial T/\partial t = 0$) involving chopped cw lasers, one may note that the spatial derivative ($\nabla^2 = \partial^2/\partial y^2 + \nabla_x^2$) imply that the temperature rise ΔT will be inversely proportional to the grating constant (and cell thickness). This point is particularly obvious if we perform a simple one-dimensional calculation, and is expected from physical grounds. This dependence was qualitatively verified in our experiment. The diffraction efficiency increases with increasing grating constant.

The experimental setup used for the observation of amplified reflection and self-oscillation is depicted in Fig. 2. The laser used is the 5145-Å line from an Ar⁺ laser. The path lengths of the beam are adjusted to be very nearly equal to optimize the interference modulation. The two laser beams are crossed at a very small angle θ on the sample (θ ranges from 1/250 to 1/350 rad). The size of the laser beam on the sample is about 2 mm. The sample used is a homeotropically aligned MBBA film with a thickness of 100 μm . The lasers are almost normally ($\beta = 0$) incident on the film, i.e., the

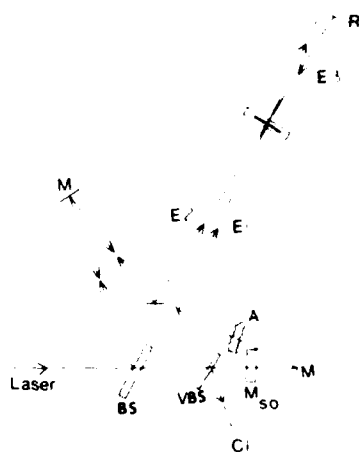


FIG. 2. Schematics of the experimental setup for observing wave front conjugation and self-oscillation. The incident laser is chopped. M: mirrors; S: sample; R: 100% reflector; BS: beam splitter; A: aberrator; VBS: variable beam splitter; M_{so} (in dotted line) is a 99% reflecting mirror to be inserted for self-oscillation effect.

optical electric field is perpendicular to the director axis. The incident probe laser power is adjusted with the variable beam splitter. The mirror M_{so} (in dotted line) when used for self-oscillation experiments, is aligned to exactly reflect the probe beam E_1 . The incident laser beam is chopped at a rate of about 4 Hz. At this rate there is an overall heating of the sample. However, this overall heating effect is just sufficient to warm the sample (from room temperature 27 °C) to near T_c (T_c of MBBA is 42 °C) when very large wave-front conjugation efficiency is obtained.

Very strong conjugated signals are observed for a wide range of probe beam powers used. At equal pump and probe power, a reflection efficiency of about 1% is observed for the sample maintained at room temperature (by using very low power pump and probe laser < 100 mW). A dramatic increase in the reflection efficiency (to more than 20 times) is observed if the temperature of the sample is raised (cf. Fig. 3) either by placing the sample in a temperature cell or by an overall heating with an increase in the laser powers to about 1 W. The reflection efficiency increases if the ratio of the pump beam power to the probe beam power is increased. At a beam ratio of about 250, and an external wave mixing angle $\theta = 1/300$ (corresponding to a wave mixing angle of 1/450 within the sample, and a grating constant $\lambda_q = 225 \mu\text{m}$), amplified reflection (> 100%) is observed. This occurs at a pump beam of 1 W, corresponding to a pump laser intensity of about 25 W/cm² on the sample.

Because of the amplified reflection capability, self-oscillation starting from noise generated in the film in conjunction with an external feedback is also possible. To observe this effect, the mirror M_{so} (99% reflecting at 5145 Å) is inserted between the variable beam splitter VBS and the mirror M. The probe beam is blocked with an opaque material between the beam splitter (BS) and VBS. With a pump power input of about 1 W, a clearly visible self-oscillation generated beam is observed in the direction along C_1 . The exit beam power at C_1 is estimated to be tens of microwatts. The self-oscillation occurs despite a strong scattering loss ($\approx 25\%$) experienced by all the beams in traversing the sample and the

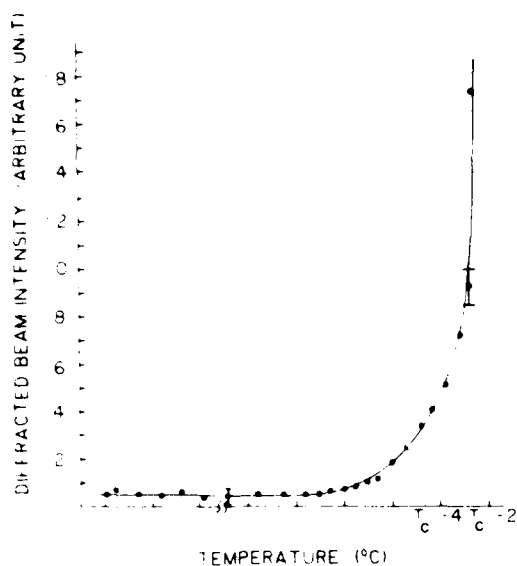


FIG. 3. Plot of the diffraction efficiency R as a function of the temperature at very low pump and probe laser power at temperature far from T_c , the diffraction efficiency is about 1%. Near T_c , it increases by about 20 times.

presence of the aberrator. Because of thermal fluctuations in the path of the lasers, and also in the liquid-crystal film itself, there is considerable instabilities in the observed self-oscillations. The oscillations appear as a highly brightened beam along C_1 (observed on a screen) that lasted several seconds, disappeared temporarily, and appeared again, very much like a cw laser just above threshold and oscillating in an open atmosphere (i.e., no enclosure to minimize the thermal instability in the air). We have also used a much more simplified setup from Fig. 2, consisting of a retroreflecting (for the pump laser) mirror and another mirror oriented to reflect the conjugated beam back to the sample.

Although MBBA possesses a significant absorption at 5145 Å, it tends to deteriorate in quality with age, as often noted by many researchers. We have experimented with the more stable liquid-crystal PCB, in which traces of dyes (R6G) are dissolved to improve the absorption rate of 5145 Å (PCB possesses very little amplified natural absorption at

5145 Å), and observed similar wave front conjugation and self-oscillation effects.

In conclusion, we have demonstrated the possibility of observing amplified reflection in wave front conjugation, and self-oscillation, using the thermal nonlinearity of a nematic liquid-crystal film. The configurations and conditions for these effects have obviously not been optimized, but the results of this and our recent studies clearly provide the basis for optimization. The effect can also be applied in constructing a ring oscillator. It is also obvious that other types of lasers (cw or pulsed) can also be used (e.g., CO₂ laser at 10.6 μm where liquid crystals also possess natural absorption, Nd:YAG laser at 1.06 μm if the liquid crystal is "doped" with traces of IR absorbing dyes, etc.). Works along these lines are currently in progress and will be reported elsewhere.

I am grateful for some technical assistance by R. R. Michael, G. Finn, and T. H. Liu. The support of the National Science Foundation (ECS 8415387) and the Air Force Office of Scientific Research (840375) is also acknowledged.

¹For a recent review see, for example, *Optical Phase Conjugation*, edited by R. Fisher (Academic, New York, 1983); see also J. F. Reintjes, *Nonlinear Optical Parametric Processes in Liquids and Gases* (Academic, New York, 1983) and all the references therein on nonlinear materials.

²See, for example, J. Feinberg and R. W. Hellwarth, *Opt. Lett.* **5**, 519 (1980); H. Rajbenbach and J. P. Huignard, *Opt. Lett.* **10**, 137 (1985); B. Fisher, M. Cronin-Golomb, J. P. White, and A. Yariv, *Opt. Lett.* **6**, 519 (1981); R. Jain and G. Dunning, *Opt. Lett.* **7**, 420 (1982); R. G. Caro and M. C. Gower, *Appl. Phys. Lett.* **39**, 855 (1981).

³See, for example, I. C. Khoo and Y. R. Shen, *Optical Engineering* **24**, 579 (1985) which provides an overview of the two types of nonlinearity.

⁴On orientational nonlinearity, see I. C. Khoo and S. L. Zhuang, *Appl. Phys. Lett.* **37**, 3 (1980); I. C. Khoo, *Phys. Rev. A* **23**, 2077 (1981); **25**, 1636 (1982); **27**, 2747 (1983); S. D. Durbin, S. M. Arakelian, and Y. R. Shen, *Phys. Rev. Lett.* **47**, 1411 (1981); H. L. Ong, *Phys. Rev. A* **28**, 2393 (1983).

⁵On thermal nonlinearity, see I. C. Khoo and S. Shepard, *J. Appl. Phys.* **54**, 5491 (1983); I. C. Khoo and R. Normandin, *IEEE J. Quantum Electron.* **QE-21**, 329 (1985); *Opt. Lett.* **9**, 285 (1984); H. Hsiung, L. P. Shi, and Y. R. Shen, *Phys. Rev. A* **30**, 1453 (1984).

⁶I. C. Khoo and S. L. Zhuang, *IEEE J. Quantum Electron.* **QE-18**, 246 (1982); E. N. Leith, H. Chen, Y. S. Cheng, G. J. Swanson, and I. C. Khoo, *Proceedings of 5th Rochester Conference on Coherence and Quantum Optics*, Rochester, June 1983.

Infrared to visible image conversion capability of a nematic liquid crystal film

I. C. Khoo

Electrical Engineering Department, The Pennsylvania State University, University Park, Pennsylvania 16802

R. Normandin

Division of Microstructural Sciences, National Research Council of Canada, Ottawa, KIA OR6, Canada

(Received 18 April 1985; accepted for publication 3 June 1985)

We present a theoretical evaluation and experimental results of the capability of a nematic liquid crystal film for infrared to visible image conversion using nondegenerate four-wave mixing process.

Degenerate and nondegenerate four-wave mixings have been studied in the context of optical imagings in several materials.^{1,2} In particular, Martin and Hellwarth¹ have demonstrated infrared to visible image conversion via Bragg reflections from laser induced thermal gratings in dyed liquids. The basic mechanism is the absorption of the incident (1R) light by the dye molecules, which then heat up the solvent via some intermolecular relaxation processes.

Recently, we have demonstrated that nematic liquid crystals possess extraordinarily large optical nonlinearity that can be utilized for wave front conjugation purposes.³ There are two distinct types of nonlinearities: thermal and orientational. Depending on the thickness of the sample and the interaction geometry between the laser polarization and the liquid crystal axes, one or both of these nonlinearities will dominate the nonlinear optical process under study.⁴⁻⁶ The thermal nonlinearity, of course, depends on the absorption constant of the liquid crystal, which can be enhanced with traces of dissolved dyes with the appropriate absorption band. A detailed analysis of the thermal nonlinearity of nematics has been performed.⁵

For incident laser polarization parallel to the nematic axis, the "extraordinary" thermal index gradient dn_{\parallel}/dT is

given by⁵

$$\frac{dn_{\parallel}}{dT} = 2n^{-1} \left((1.33 + 0.74S) \frac{d\rho}{dT} + 0.74 \frac{dS}{dT} \right). \quad (1)$$

And for the incident laser polarization perpendicular to the nematic director axis, the "ordinary" thermal index gradient dn_{\perp}/dT is

$$\frac{dn_{\perp}}{dT} = 2n^{-1} \left((1.33 - 0.37S) \frac{d\rho}{dT} - 0.37 \frac{dS}{dT} \right) \quad (2)$$

for PCB (pentyl-cyano-biphenyl), where S is the temperature-dependent order parameter and ρ is the density. A unique characteristic of nematic liquid crystals is the rather large magnitudes of both dn_{\parallel}/dT and dn_{\perp}/dT . At temperatures far away from the nematic isotropic transition temperature (e.g., at 22 °C and $T_c = 35$ °C for PCB), both dn/dT 's are already comparable to the largest thermal index obtainable in liquids ($\sim 10^{-4} \text{ K}^{-1}$). At temperatures closer to T_c , both dn_{\perp}/dT and dn_{\parallel}/dT increase dramatically by more than an order of magnitude. This means that thinner samples and/or low power lasers can be used for optical wave mixing processes, since the diffraction efficiency is proportional to the square of dn/dT , among other factors. In

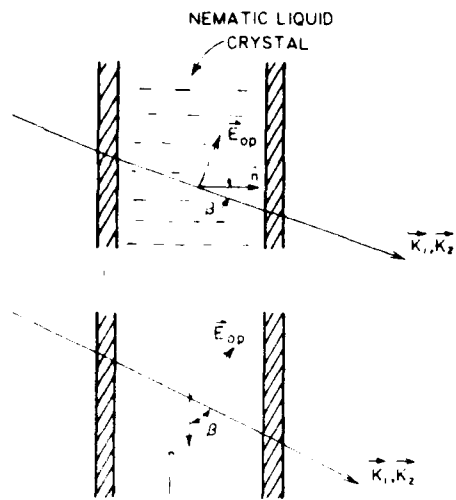


FIG. 1. (a) Homeotropically aligned nematic liquid crystal. (b) Planar nematic liquid crystal. \mathbf{K} and \mathbf{E}_{0p} are the wave vector and electric field vector of the laser, respectively. For $\beta = 0$, \mathbf{E}_{0p} is parallel to \mathbf{n} . For $\beta = 90^\circ$, \mathbf{E}_{0p} is perpendicular to \mathbf{n} , the director axis of the nematic. \mathbf{K}_1 and \mathbf{K}_2 are crossed on the sample at 3° .

particular, because of the thinner sample geometry, one expects to get higher resolution element capability in infrared to visible image conversion process as we will explain presently.

Another unique characteristic of liquid crystals is the extraordinarily large optical nonlinearity associated with molecular reorientation. Molecular reorientation of nematic liquid crystal axis is of course wavelength independent which makes it the most versatile and natural mechanism for image conversions (IR to visible, ..., etc.). The optical nonlinearity associated with two lasers (pump-probe) intersecting on the liquid crystals has been calculated before. The in-

duced optical refractive index change is given by⁴

$$\delta n \sim \frac{1}{2} \frac{\delta \epsilon}{n} = \frac{\epsilon_i \Delta \epsilon}{2n\epsilon_1} \sin 2\beta \theta, \quad (3)$$

where θ is the optically induced molecular reorientation. The nonlinearity can be induced in homeotropic or planar aligned nematic liquid crystal films for the optical field-nematic interaction geometries depicted in Figs. 1(a) and 1(b). In general, the molecular reorientational nonlinearity is larger than the thermal nonlinearity. However, it is obvious that for $\beta = 0$, the reorientational nonlinearity is vanishing.

We have experimentally demonstrated the possibility of infrared to visible image conversions in pure nematic films and also in nematic films "doped" with infrared absorbing dyes. The liquid crystal used is PCB (4-cyano-4'-pentyl-biphenyl) and is about $50 \mu\text{m}$ thick. Both homeotropically aligned and planar nematic films have been shown to give similar results. The sample temperature is 22°C . Various four-wave mixing (wave vectors) configurations have been attempted. Figure 2(a) shows one of the setups used, with all four waves propagating in the forward direction [cf. Fig. 2(b)]. A 20-ns Nd:YAG laser pulse (λ at $1.06 \mu\text{m}$) is split into the reference beam and an object beam (the object is a wire mesh). These two beams recombine on a homeotropically aligned nematic film at an angle of about 3° . The lasers are linearly polarized, with the polarization normal to the director axis. For this geometry, the nonlinearity comes from dn_1/dT . Traces of Kodak No. 14015 infrared absorbing dyes were dissolved in the liquid crystal to improve the absorption of the PCB at $1.06 \mu\text{m}$. A cw 5-mW He-Ne ($0.6328 \mu\text{m}$) laser is used as a reconstruction beam and is almost collinear with the reference beam. The beam spot sizes on the liquid crystal film are on the order of 0.5 cm^2 . Visible diffraction values of the He-Ne were observed for reference beam

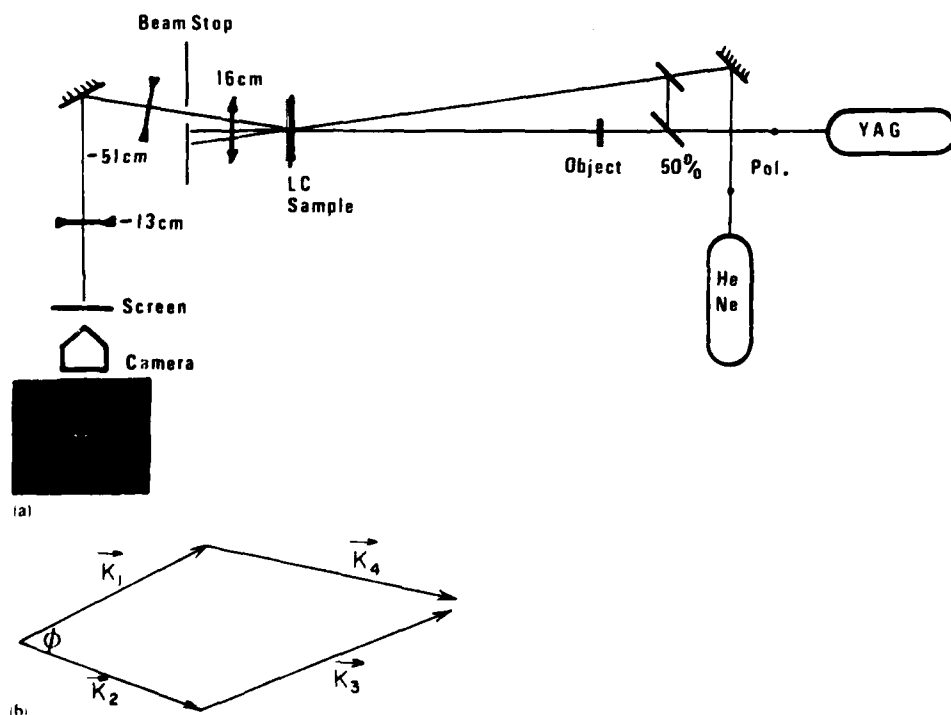


FIG. 2. (a) Schematic of the experimental setup. Photo insert is a sample experimental result. (b) Wave vector configuration of the reference (\mathbf{K}_1), the object (\mathbf{K}_2), the reconstructing (\mathbf{K}_3), and the image beams (\mathbf{K}_4).

and object beam energies on the order of 50 and 15 mJ, respectively. The observed diffraction efficiency is on the order of a few percent. The diffracted image beam is imaged via the lens system onto the Polaroid film plate. In general, very good quality image can be reconstructed. The photo insert in Fig. 2 shows a typical reconstructed image of the mesh at the red wavelength (0.6328 μm).

The diffraction efficiency of the 50- μm -thick film is very good, and is on the order of a few percent (as measured from the diffraction from the 1R laser pulses with a joulemeter). In Ref. 1, it was reported that similar diffraction efficiency was observed in a 2-mm-thick dye solutions, using pump and probe beam energies on the order of 10 and 1 mJ, respectively, focused on an area of about 0.01 cm^2 . In comparison to these liquids, the higher efficiency of the nematic film due to its inherently higher dn/dT is already evident.

The thickness of the nematic film ($\approx 50 \mu\text{m}$) means that higher resolution elements can be achieved. For the geometry depicted in Fig. 2(b), and using an analysis similar to Martin and Hellwarth, the number of resolution elements, N , can be proven in a straightforward manner to be given by

$$N = \frac{AK_1/l}{1 + K_1/K_2} \quad (4)$$

in the small ϕ limit (i.e., $\phi \ll 1$). This differs from the "folded" geometry used by Martin and Hellwarth by the denominator, where it is replaced by $[1 - K_1/K_2]$. Since $K_1 = 2K_2$, the difference between N here and N in Ref. 1 is a factor of 1/2 to 3/2, i.e., N here is smaller than N in Ref. 1 by a factor of 3. On the other hand, the thickness l in the present case (50 μm) is much smaller than (by a factor of 40) the 2-mm cell thickness. Using thinner cell for higher resolution element is, of course obvious, but the important point here is that one can get comparable diffraction efficiencies even with such thin films. The efficiency obtained here is by no means optimized. We have observed that the diffraction efficiency increased by at least an order of magnitude by raising the temperature of the sample to near T_c (30 $^\circ\text{C}$).

To demonstrate the use of the other type of nonlinearity, namely, orientational nonlinearity, we use a *pure* PCB film (same thickness of 50 μm). The sample does not give visible diffractions even at much higher input laser energies than the ones used in the above experiment involving dyed samples. The sample is tilted such that β , the propagation angle which the wave vector \mathbf{K}_1 (\mathbf{K}_2) makes with the nematic axis, is 22 $^\circ$ (cf. Fig. 1). An almost cw beam of Nd:YAG pulses is obtained by running the laser at 20 pps. This continuous illumination is required simply because the orientational response of the nematic is slow (on the order of milliseconds).

In this case, we also observe visible diffraction of the He-Ne beam and images of comparable quality. To check that indeed the mechanism is due to orientational effect, the film is tilted back to the normal position (i.e., $\beta = 0$) and the diffraction vanishes [in accordance to Eq. (3)]. Due to pulse to pulse instabilities, the effects for cw laser are not as large and the quality of the image is not as good as expected. It is clear that better results can be obtained if one uses a cw laser or millisecond 1R laser pulses.

The temporal behaviors of the thermal and orientational gratings are quite different. Using an almost identical setup as Fig. 2(a) (with the object removed), we have measured the rise time of the thermal grating by detecting the diffraction from the He-Ne laser. In general, the rise time is on the order of the Nd:YAG pulse width (≈ 20 ns), while the decay time is on the order of 50–100 μs , depending on various parameters but mostly on the grating spacing. On the other hand, the rise time associated with molecular reorientation is much slower. Under cw excitation, the rise time is on the order of 10^2 ms, and becomes shorter at higher incident laser intensity (very similar to liquid crystal reorientation by dc field).⁷ The decay time is also on the order of 10^2 ms, and depends primarily on the grating constant and/or film thickness.

In conclusion, we have demonstrated the possibility of infrared to visible image conversion. Without optimization, the results are comparable to those achievable in much thicker high thermal index liquids. We are currently investigating the details of this process with respect to various parameters, e.g., laser pulse length, absorption constants, geometry, etc., and will report the result in a longer article elsewhere.

This research is supported by a grant from the National Science Foundation ECS 8415387 and from the Air Force Office of Scientific Research under AFOSR 840375.

¹G. Martin and R. W. Hellwarth, *Appl. Phys. Lett.* **34**, 371 (1979).

²J. F. Reintjes, *Nonlinear Optical Parametric Processes in Liquids and Gases* (Academic, Orlando, 1984) and references therein on degenerate four-wave mixings, Chaps. 5, 6.

³I. C. Khoo and S. L. Zhuang, *IEEE J. Quantum Electron.* **QE-18**, 246 (1981); E. N. Leith, H. Chen, Y. Cheng, G. Swanson, and I. C. Khoo, *Proceedings of 5th Rochester Conference on Coherence and Quantum Optics*, June 1983, Rochester, N.Y.

⁴I. C. Khoo, *Phys. Rev. A* **25**, 1637 (1982); **27**, 2747 (1983).

⁵I. C. Khoo and R. Normandin, *IEEE J. Quantum Electron.* **QE-21**, 329 (1985); I. C. Khoo and R. Normandin, *Opt. Lett.* **9**, 285 (1984).

⁶I. C. Khoo and Y. R. Shen, *Opt. Eng. Special Issue*, July (1985).

⁷P. G. deGennes, *The Physics of Liquid Crystals* (Oxford University, Oxford, England, 1974).

END

10-86

DTIC